Published in final edited form as:
Pharm Res. 2015 March ; 32(3): 1028–1044. doi:10.1007/s11095-014-1515-z.

Peripherally cross-linking the shell of core-shell polymer micelles decreases premature release of physically loaded combretastatin A4 in whole blood and increases its mean residence time and subsequent potency against primary murine breast tumors after IV administration

Rajesh R. Wakaskar[2], **Sai Praneeth R. Bathena**[2], **Shailendra Tallapaka**[2], **Vishakha V. Ambardekar**[3], **Nagsen Gautum**[2], **Rhishikesh N. Thakare**[2], **Samantha M. Simet**[4], **Stephen M. Curran**[2], **Rakesh K. Singh**[1,5], **Yuxiang Dong**[2], and **Joseph A. Vetro**[1,2]

[1]Center for Drug Delivery and Nanomedicine, College of Pharmacy, University of Nebraska Medical Center, 986025 Nebraska Medical Center, Omaha, Nebraska 68198-6025, USA

[2]Department of Pharmaceutical Sciences, College of Pharmacy, University of Nebraska Medical Center, 986025 Nebraska Medical Center, Omaha, Nebraska 68198-6025, USA

[3]Nanotechnology Characterization Laboratory, Cancer Research Technology Program, Leidos Biomedical Research, Inc., Frederick National Laboratory for Cancer Research, Frederick, MD-21702, USA

[4]Department of Pulmonary, Critical Care, Sleep, & Allergy, College of Medicine, University of Nebraska Medical Center, 981050 Nebraska Medical Center, Omaha, Nebraska 68198-1050, USA

[5]Department of Pathology and Microbiology, University of Nebraska Medical Center, 985900 Nebraska Medical Center, Omaha, NE 68198-5900, USA

Abstract

Purpose—Determine the feasibility and potential benefit of peripherally cross-linking the shell of core-shell polymer micelles on the premature release of physically loaded hydrophobic drug in whole blood and subsequent potency against solid tumors.

Methods—Individual Pluronic F127 polymer micelles (F127 PM) peripherally cross-linked with ethylenediamine at 76% of total PEO blocks (X-F127 PM) were physically loaded with combretastatin A4 (CA4) by the solid dispersion method and compared to CA4 physically loaded in uncross-linked F127 PM, CA4 in DMSO *in vitro*, or water-soluble CA4 phosphate (CA4P) *in vivo*.

Results—X-F127 PM had similar CA4 loading and aqueous solubility as F127 PM up to 10 mg CA4 / mL at 22.9 wt% and did not aggregate in PBS or 90% (v/v) human serum at 37°C for at least 24 h. In contrast, X-F127 PM decreased the unbound fraction of CA4 in whole blood (*fu*) and increased the mean plasma residence time and subsequent potency of CA4 against the vascular

Correspondence to: Joseph A. Vetro.

function and growth of primary murine 4T1 breast tumors over CA4 in F127 PM and water-soluble CA4P after IV administration.

Conclusions—Given that decreasing the fu is an indication of decreased drug release, peripherally cross-linking the shell of core-shell polymer micelles may be a simple approach to decrease premature release of physically loaded hydrophobic drug in the blood and increase subsequent potency in solid tumors.

Keywords

drug delivery; polymer nanocarriers; Pluronic F127; poloxamer 407; premature drug release; peripheral shell cross-linking; vascular disrupting agents

INTRODUCTION

The IV route of administration provides several advantages for the pharmacotherapy of cancer with low MW drugs (~500 Da) including maximum bioavailability, rapid drug action, and the option to tightly control and maintain therapeutic concentrations of drug in the blood for an extended duration through IV infusion (1). The IV administration of hydrophobic, low MW drugs with poor aqueous solubility (<50 μg/mL) (2), however, can lead to the formation of drug aggregates in the blood that potentially cause respiratory failure (3), increase local drug toxicity, and decrease bioavailability (4). This is especially problematic for conventional IV formulations that use co-solvents or adjust the pH to increase aqueous drug solubility because solution conditions likely change significantly after IV administration (2). These same formulations may also cause pain, phlebitis, inflammation, hemolysis, and/or unacceptable levels of toxicity upon injection and can be dose-limiting (2).

Core-shell polymer micelles (PM) are being widely developed as an alternative, less toxic approach to improve the IV administration of low MW drugs with poor aqueous solubility (5, 6). The most developed core-shell PM are formed from amphiphilic diblock (hydrophilic-hydrophobic) copolymers or triblock (hydrophilic-hydrophobic-hydrophilic) copolymers (7–9) such as Pluronic F127 (poloxamer 407) (8) that spontaneously self-assemble into spherical, nano-sized micelles when the unimers are directly or indirectly dissolved in aqueous solution above a threshold concentration (critical micelle concentration, CMC) and solution temperature (critical micelle temperature, CMT) (5) (Fig. 1A). Core-shell PM then consist of a hydrophobic core for drug loading and a hydrophilic shell to prevent the aggregation of PM before and after IV administration and, ideally, protect loaded drug while localizing to the site of drug action (5).

Hydrophobic, low MW drugs can be loaded into core-shell polymer micelles by chemically conjugating the drug to the hydrophobic block before self-assembly (10–14) or by physically loading the drug into the hydrophobic core during or after self-assembly (5). Physical loading is generally preferred over chemical conjugation, however, because higher levels of drug loading are possible (15) and because many drug molecules must be additionally modified to facilitate chemical conjugation (5), whereas the hydrophobic block

can be easily modified to increase physical drug loading without changing the original drug molecule (16–18).

In addition to increasing aqueous solubility with less formulation toxicity, core-shell PM ideally increase the bioavailability of loaded drug after IV administration (6) and potentially increase the potency of loaded drugs against solid tumors by increasing passive accumulation at the tumor site due to leaky tumor vasculature (19). Differences between pharmacokinetic profiles from clinical trials with doxorubicin physically loaded into mixed core-shell PM of Pluronic F127/L61 (20) or PEGylated liposomes (21), however, suggest that drugs physically loaded into core-shell PM have the potential to be prematurely released after IV administration (22).

Given that IV administration highly dilutes core-shell PM to concentrations well below the CMC of most polymers used for drug delivery, PM disassembly is generally assumed to be the primary cause of premature drug release (20, 22–24). Preventing the presumed PM disassembly by cross-linking core-shell PM through functional groups within the core-forming block (Fig.1B, core cross-linking) or through functional groups within the shell-forming block (Fig.1B, internal shell cross-linking) (24–27) can increase the bioavailability and, in some cases, the potency of physically loaded drugs against solid tumors relative to uncross-linked PM after IV administration (28–30) but may also decrease drug loading and the rate of drug release at the target cell (24). Cross-linking the shell of core-shell PM through peripheral functional groups on the shell surface (Fig.1B, peripheral shell cross-linking) may have similar effects on the bioavailability and potency of physically loaded drug but with less effect on drug loading, drug release at the target cell, and/or the functionality of the PM shell after IV administration. The feasibility and potential of this approach, however, has not been fully explored. In this study, we highly cross-linked the shells of individual Pluronic F127 PM with ethylenediamine through peripheral hydroxyl end-groups to a maximum of 76% of total PEO blocks (X-F127 PM), physically loaded a model, hydrophobic low MW drug (combretastatin A4 [CA4]) by the solid dispersion method, and compared CA4 loaded in X-F127 PM to CA4 loaded in uncross-linked F127 PM, CA4 solubilized in water with DMSO (*in vitro*), or water-soluble CA4 phosphate [CA4P] (*in vivo*).

MATERIALS AND METHODS

Peripheral shell cross-linking of Pluronic F127 PM

Unless otherwise indicated, all reagents were from Sigma (St. Louis, MO) and all steps were performed at room temperature (r.t.). Pluronic F127 (F127 [5 g, 397 μmol]) was dissolved in anhydrous dimethyl sulfoxide (DMSO [0.1% max. H_2O], 30 mL) in a flat-bottomed flask (250-mL). The terminal hydroxyl groups of F127 were activated by adding N,N'-disuccinimidyl carbonate (DSC [5.12 g, 20 mmol], A.K. Scientific, Inc.) to the F127 solution, stirring the uncovered solution under N_2 flow for 1 h to release CO_2 while preventing the absorption of ambient water vapor by DMSO, then capping the flask and stirring at r.t. for 3 days. The reaction was quenched by incubating the flask in iced water and adding dH_2O (10 mL) drop-wise, then stirring at r.t. for 1 h until a clear solution was formed. Water was evaporated from the quenched reaction mixture by adding acetone (50

mL) and stirring the solution at r.t. for 1 h. NHS-F127 was precipitated by adding the quenched reaction mixture drop-wise to anhydrous diethyl ether (50 mL [0.030% max. H_2O) under stirring.

The precipitate was collected by filtration (Whatman Grade I Filter Paper), washed with anhydrous diethyl ether (50 mL), dialyzed (Snake Skin dialysis tubing, 10 kDa MWCO, Thermo Scientific) against 100% EtOH (3 × 5 L over 12 h), dried under a fume hood for 1 day, and stored at −20°C in a glass jar sealed with parafilm. NHS-F127 polymer micelles (NHS-F127 PM) were formed by equilibrating a solution of NHS-F127 (315 mg, 25 μmol) in MES buffer (Sodium MES in dH_2O [0.05 M, pH 6.0], 12.5 mL) at r.t. for 10 min then dividing aliquots (5 × 2.5 mL) into 20-mL glass vials. NHS-F127 PM were cross-linked by adding a solution of ethylenediamine (ED) in MES buffer (2.5 mL) to each aliquot of NHS-F127 PM at the indicated molar ratio of ED/NHS-F127, incubating capped vials with stirring for 2 h, dialyzing (Snake Skin dialysis tubing, 10 kDa MWCO, Thermo Scientific) against dH_2O (4 × 5 L over 24 h), lyophilizing for 2 days, and storing at −20°C in a glass vial sealed with parafilm. The hydrolytic stability of NHS-F127 under these reaction conditions was determined by ^{1}H-NMR (500 MHz, $CDCl_3$, 1 mg/mL) comparing the ratio of the area of protons at 2.85 ppm that represent NHS (Fig.S1A, peak 2) relative to the area of protons at 1.26 ppm that represent F127 (Fig.S1A, peak 5) before and after incubation under reaction conditions in the absence of ED.

Extent of Pluronic F127 PM cross-linking with ethylenediamine

The extent of F127 PM shell cross-linking with ethylenediamine was determined by ^{1}H-NMR (500 MHz, $CDCl_3$, 1 mg/mL) by subtracting the peak area of protons at 3.12 ppm that represent the monovalent attachment of ED (Fig.S1B, peak 4) from the peak area of protons at 4.22 ppm after reaction with ED that represent both monovalent and divalent (i.e., cross-linking) ED conjugation to F127 PM (Fig.S1B & C, peak 1A) and dividing by four (the area of the 4.22 ppm peak expected with 100% divalent ED conjugation) where percent F127 PM cross-linking = [Peak area$_{4.22\ ppm}$ - Peak area$_{3.12\ ppm}$] / 4 × 100. The average percent of total F127 PEO blocks cross-linked with ED ± SD (n=2 from the same batch) vs. molar ratio of ED/NHS-127 was fit by a second-order polynomial ($Y = B_0 + B_1X + B_2X^2$) using GraphPad Prism 6.

Sizing of F127 PM in PBS and human serum

The hydrodynamic diameters of the polymer micelles were determined by DLS (Malvern ZS90). A clear stock solution was obtained by dissolving lyophilized samples in PBS (20 mg/mL) and vortexing for 10 sec. The stock solution (0.1 mL) was diluted 1/10 by adding to PBS [pH 7.4] (0.9 mL) or human serum (Gemini Bioproducts, 0.9 mL), vortexed for 10 sec, and incubated in a water bath at 37°C for 2 h or 24 h as indicated. Average hydrodynamic diameters ± SD (n = 3 from the same batch) were compared by one way ANOVA with Tukey post-test.

Sizing of lyophilized F127 PM

The diameters and heights of lyophilized F127 PM were determined by Atomic Force Microscopy (Ntegra-Spectra, NT-MDT). Samples were prepared by dissolving lyophilized

formulations in PBS (10 mg/mL), incubating in a sonication bath for 5 min, diluting 1/1 (10 μL sample + 10 μL PBS), incubating sample solutions (20 μL) on Mica strips previously modified with aminopropyl silane (APS) for 2 min, washing the strips with dH_2O (0.2 mL), then drying under ambient conditions. Sample strips were attached to a glass slide with adhesive tape and imaged. Average diameters and heights ± SD and H/D ratios ± propagated SD (n = 30 micelles from the same batch) were obtained from the Height or Amplitude Image using the Femtoscan software and fit vs. average percent ED cross-linking ± SD (n=2) using GraphPad Prism 6.

Combretastatin A4 (CA4) loading in F127 PM by the solid dispersion method

F127 PM were loaded with Combretastatin A4 (CA4; CAS# 82855-09-2; Topharman LLC, USA) using an adaptation of the solid dispersion method (31). For CA4 loading at 12.9 wt %, CA4 (20 mg) then F127 (135 mg) was dissolved in ethanol (200 proof, 3 mL) and stirred at 37°C for 30 min. CA4 loading was increased to 22.9 wt% by using double the mass of CA4 (40 mg) or half the mass of F127 (67.5 mg) in the solid dispersion as indicated. Ethanol was evaporated under a fume hood until a dry, crusty white powder was formed before dH_2O (40 mL) was added to the beaker and stirred at 60°C for 2 h. Solutions were cooled to r.t. and undissolved CA4 was pelleted (10,000 RCF, 50-mL Oakridge Centrifuge tubes, 10 min). Supernatants were transferred to glass beakers, flash-frozen with liquid N_2, incubated at −80°C for 30 min, then lyophilized (Labconco) for 2 days before storage at −20°C. CA4 loading in the lyophilized formulations was determined by LC-MS/MS after dissolving in ethanol (200 Proof Spectrophotometric Grade, 0.1 mL) at a theoretical concentration of 10 mg CA4/mL, diluting 1/10,000 in ethanol, then diluting 1/10 in 80% acetonitrile (95.5% ACS Grade, max. water < 0.3%) to 100 ng CA4/mL theoretical. Samples were analyzed with a Waters ACQUITY UPLC system (Waters, Milford, MA) coupled to an Applied Biosystems 4000 Q TRAP® quadrupole linear ion trap hybrid mass spectrometer with an electrospray ionization (ESI) source (Applied Biosystems/MDS Sciex, Foster City, CA) controlled by Empower Pro 6.0 and Analyst 1.4.2 software, respectively. Chromatographic separations were performed using an ACQUITY UPLC® BEH Shield RP18 column (1.7 mm, 100 mm × 2.1 mm) equipped with an ACQUITY UPLC® C18 guard column (Waters, Milford, MA). The mobile phase was 55% acetonitrile (ACN) and 45% of 0.2% acetic acid at a total flow rate of 0.3 ml/min and samples (10 μL) were injected with an autosampler. CA4 was quantified in the negative ionization mode with the following mass spectrometer source settings: ion spray voltage, −4500 V; source temperature, 500 °C; curtain gas (nitrogen), 20 (arbitrary units), gas-1, 30, gas-2, 20 (arbitrary units), collision gas pressure, medium; Q1/Q3 resolution, unit; and interface heater, on. A multiple reaction monitoring (MRM) transition of 315.1 to 284.8 m/z was used with the following optimum MS parameters: declustering potential, −60 V; entrance potential, −10 V; collision energy, −28 eV; and cell exit potential, −5 V. These conditions gave a CA4 retention time of 1.8 min, narrow peak shape, high MS signal sensitivity, and a linear calibration curve from 0.1–1000 ng CA4/ml (data not shown). Averages ± SD (n = 3 from the same batch) were compared by one way ANOVA with Tukey post-test.

Aqueous solubility of CA4 loaded in F127 PM

The aqueous solubility of CA4 loaded in F127 PM was determined by LC-MS/MS as described above except that lyophilized formulations were dissolved in dH_2O (1 mL) to yield a theoretical concentration of 1 mg CA4/mL (data not shown) or 10 mg CA4/mL based on actual CA4 loading and diluted to yield CA4 concentrations within the range of the calibration curve. Average mg CA4/mL ± SD (n = 3 from the same batch) was compared by one way ANOVA with Dunnet's post-test vs. F127 PM at 12.9 wt%.

Potency of loaded CA4 against HUVEC growth *in vitro*

The potency and cytotoxicity of CA4 against human umbilical vein endothelial cells (HUVEC) was determined by cell counting with trypan blue. HUVEC were grown and treated at 37°C, 5% CO_2. CA4 was loaded in F127 PM or X-F127 PM at 22.9 wt% theoretical as described above or solubilized in dimethyl sulfoxide (DMSO Cell Culture Grade). CA4 stock solutions (400X) were prepared in PBS (F127 PM and X-F127 PM stock solutions were based on actual CA4 loading determined as described above and diluted in growth media (Vascular Cell Basal Medium plus VEGF [ATCC]) to form CA4 treatment solutions at 0, 5 nM, 50 nM, 100 nM, 5 μM, 5 μM, and 10 μM CA4. HUVEC (Passage 3, ATCC) were grown to confluence, plated in a 24-well plate (20,000 cells/well in 0.5 mL growth media), incubated for 24 h, then treated with CA4 by replacing growth media with CA4 treatment solutions (0.5 ml), incubating 4 h, replacing CA4 treatment solutions with fresh growth media (0.5 mL), and incubating an additional 24 h. HUVEC were then washed with PBS (1 mL, 3X), incubated with Accutase (0.5 mL) at 37°C for 10 min, resuspended in growth media (0.5 mL), pelleted (400 RCF, 10 min), resuspended in growth media (50 μL), diluted 1/1 with 0.2 % Trypan blue solution in PBS (50 μL), and the cell number and percent viability was determined (Cellometer Auto T4; Nexcelom Biosciences, Lawrence, MA). An average IC_{50} ± SEM (n=3 wells) was calculated by log [CA4] vs. %HUVEC growth inhibition (normalized to untreated HUVEC) using a variable slope (GraphPad Prism 6).

Activity of CA4 against HUVEC *in vitro* as monitored by electrical cell impedance substrate (ECIS)

The resistance of HUVEC after various treatments *in vitro* was monitored in real time by electric cell-substrate impedance sensing (ECIS; Applied BioPhysics, Troy, NY). The wells of an ECIS array (8W10E+, Applied Biophysics, Inc.) were prepared by incubating each well with a cysteine solution (10 mM, 0.2 mL) for 10 min, rinsing with sterile distilled water (2 × 0.4 mL), adding growth media (Vascular Cell Basal Medium plus VEGF [ATCC], 0.4 mL), and monitoring the resistance at a frequency of 4000 Hz until the signal from all wells was stable (~10 min). Growth media was removed and the wells were incubated with 0.1% gelatin (0.4 mL) at 37°C, 5% CO_2 for 30 min. The gelatin coating solution was removed from the wells and HUVEC were plated (8000 cells per well) at the same surface density as the potency studies described above. Growth media alone was added to wells 1 and 2 to control for background well resistance. The array was attached to an ECIS station and the resistance was measured every 5 min at multiple frequencies until stable (~24 h). The array was removed from the ECIS station, the indicated treatment solutions were added to each well, and the array was reattached to ECIS station and the resistance monitored for 4 h. The

array was removed to replace the treatment solutions with fresh growth media, reattached to the ECIS station, and the resistance was monitored for an additional 48 h. Cell resistance measurements were based on changes in resistance/capacitance to current flow applied to the electrode arrays at multiple frequencies. A frequency scan was performed to determine the frequency at which the largest difference in transepithelial resistance (TER) values were obtained between HUVEC-covered and HUVEC-free electrodes. Average resistance (n = 2 on each array) was normalized by dividing the resistance from treatment wells by the resistance from wells containing media only using the ECIS software.

CA4 plasma partition (*fu* assay)

The unbound fraction of CA4 in human whole blood (*fu*) was determined by an erythrocyte vs. buffer or plasma partitioning method (32). The packed cell volume of erythrocytes in human whole blood (Biochemed Services, 1 mL) was first determined using packed cell volume centrifuge tubes (Techno Plastic Products AG, Switzerland) (~40% v/v). For each condition, plasma (supernatant) and erythrocytes (pellet) from pooled, human whole blood (1 mL) were first separated (2500 RCF, 10 min) into two 1.5-mL polystyrene tubes. Erythrocytes were washed by adding PBS (1 mL), pelleting (2500 RCF, 10 min), and discarding the supernatant (3X). Plasma was added back to the washed erythrocytes (0.6 mL) to maintain a 40% (v/v) packed cell volume of erythrocytes and vortexed for 1 min. CA4 alone (1 mg CA4/mL in DMSO, 10 μL) or loaded at 22.9 wt% CA4 in F127 PM or X-F127 PM (1 mg CA4/mL in PBS, 10 μL) was added to the suspension, vortexed for 2 min, and incubated in a 37°C water bath for 1 h. The suspension was vortexed again for 2 min and an aliquot (0.1 mL) was taken that represents the concentration of CA4 in the blood cell-plasma suspension (C_B). The erythrocytes were pelleted (2500 RCF, 10 min) and an aliquot (0.1 mL) was taken from the supernatant that represents the concentration of CA4 in plasma (Cp). The same procedure was repeated with pooled, human whole blood but PBS was added to washed erythrocytes instead of plasma. For these conditions, an aliquot (0.1 mL) was taken that represents the concentration of CA4 in the blood cell-buffer suspension (C_B*). The erythrocytes were pelleted (2500 RCF, 10 min) and an aliquot (0.1 mL) was taken from the supernatant that represents the concentration of CA4 in buffer (Cb). Acetonitrile (max 0.3% water, 1 mL) was added to all aliquots and each sample was vortexed thoroughly for 2 min. Supernatants (5000 RCF, 10 min) were collected and remaining acetonitrile was evaporated. The residues were reconstituted in 80% acetonitrile in dH_2O (1 mL), vortexed thoroughly, and diluted 1/10 with 80% acetonitrile (0.1 mL sample + 0.9 mL 80% acetonitrile) and analyzed by LC-MS/MS as described above. Standards were prepared by spiking blood, plasma, buffer, and 80% acetonitrile solution (0.1 mL each) with a stock CA4 solution (100 μg CA4/mL, 10 μL) and analyzed by LC-MS/MS as described for the samples. The concentration of CA4 associated with erythrocytes in the erythrocyte-plasma samples (C_E) was calculated by:

$$C_E = \frac{C_B - Cp(1 - HCT)}{HCT}$$

where C_B is the concentration of CA4 in the erythrocyte-plasma suspension and Cp is the concentration of CA4 in plasma, and HCT is the hematocrit value (40% packed volume of

erythrocytes (v/v) = 0.4). The concentration of CA4 associated with erythrocytes in the erythrocyte-buffer samples (C_E*) was calculated by:

$$C_E* = \frac{C_B* - Cb(1 - HCT)}{HCT}$$

where C_B* is the concentrations of CA4 in the erythrocyte-buffer suspension, Cb is the concentration of CA4 in buffer, and HCT is the hematocrit value (40% packed volume of erythrocytes (v/v) = 0.4). The partition coefficients for erythrocyte-plasma (P_P) and erythrocyte-buffer (Pb) were calculated from C_E and C_E* by:

$$P_p = \frac{C_E}{Cp}$$

$$Pb = \frac{C_E*}{Cb}$$

The unbound drug fraction (*fu*) (% of free drug) was then calculated from PP and Pb by:

$$fu(\%) = \frac{P_p}{Pb} \times 100$$

Average *fu* ±SD (n=3) were compared by one way ANOVA with Tukey post-test.

Activity of CA4 against tumor vascular function and tumor growth

All procedures were approved by the University of Nebraska Medical Center Institutional Animal Care and Use Committee. The extent of vascular shutdown and growth inhibition of primary tumors was determined by an IVIS-based method (33) and monitoring tumor volumes, respectively. 4T1 cells stably expressing luciferase (4T1-Luc) (34) were injected s.q. (1 × 10 cells in 0.1 mL sterile PBS) into the mammary fat pads of female BALB/c mice (6–8 weeks, NCI) and tumor volumes were measured daily by Vernier calipers where tumor volume = (a^2 x b)/2 and perpendicular tumor diameter a > b. On the day of treatment (~100 mm^3 tumor volume), a baseline luciferase signal from primary 4T1-Luc tumors was established at t = 0 by anesthetizing the mice with 1% isoflurane and measuring average radiance (photons/sec/cm^2 /sr) by IVIS [Emission filter = Open, Bin: (M)8, Field of View: 23.6, f4, exposure time: 60 sec] 15 min after injecting D-Luciferin i.p. (30 mg/mL in 0.1 mL PBS). Immediately after imaging, PBS, water-soluble CA4 phosphate (CA4P; CAS# 168555-66-6; Topharman LLC, USA), or CA4 loaded in F127 PM or X-F127 PM at 22.9 wt % as described above was injected in the tail vein at 1 mg CA4 / kg (200 μg CA4 / mL in sterile PBS, 0.1 mL). Average radiance was then determined 2, 6, and 24 hr after IV injection by injecting D-Luciferin i.p. and measuring by IVIS. Average percent vascular shutdown ± SD (n = 6 mice) at each time point was calculated [100 – ((average radiance at t = 0 / average radiance at t = 0 + n) x 100))] and compared to PBS treatment by Kruskal-Wallis nonparametric ANOVA with Dunn's post-test.

Pharmacokinetics and distribution of CA4

The pharmacokinetics and distribution of CA4 in tumor-bearing mice was determined by LC-MS/MS. Tumors of 4T1-Luc were grown to ~100 mm^3 and water-soluble CA4 phosphate (CA4P) or CA4 loaded in F127 PM or X-F127 PM at 22.9 wt% was injected as described above. Blood (~0.1 mL) from treated and untreated mice (matrix controls) was collected into Li-heparinized tubes (0.3 mL Microvette Tubes, Sarstedt) from a submandibular bleed (5 mm Goldenrod lancet, Braintree Scientific) at 5 min, 1 h, and 2 h post-injection before organ collection at 2 h or 15 min, 6 h, and 12 h post-injection before organ collection at 24 h (n = 6 mice per time point), and plasma supernatants (3000 RCF, 10 min) were stored at −80°C. The indicated organs & tumors were collected from treated and untreated mice (matrix controls) by euthanizing (isoflurane drop jar/cervical dislocation), rinsing organs in dH_2O (dipped 1X in a series of three beakers filled with 50 mL dH_2O), blotting on Kim wipes, weighing, and storing at −80°C. Organs homogenates were prepared by adding 4 vol. of dH_2O to 1 vol. thawed tumors/organs (w/w), completely homogenizing (PowerGen 500 with dH_2O / EtOH rinses between samples, 10,000 rpm), and storing at −80°C. For drug extraction, acetonitrile [ACN] (1 mL) was added to thawed plasma (50 μL) or tumor/organ homogenate (100 μL), vortexed 30 sec, mixed with an orbital shaker at r.t. for 2 h, pelleted (10,000 RCF at 4°C for 10 min), and ACN removed by a Speedvac concentrator (medium setting overnight). Calibration curves (0.5, 1, 2, 5, 10, 20, 50, 100, 500, 1000 ng CA4 / mL final conc.) were generated by adding 10X CA4 stock solutions in DMSO (10 μL) to thawed plasma (50 μL) or tumor/organ homogenates (0.1 mL) from untreated mice and extracting drug as described for treated mice (Table S4). CA4 recoveries ranged from 80% to 120% within the linear range of the standard curve. All samples were reconstituted in ACN (80% v/v in dH_2O, 0.1 mL), vortexed 30 sec, pelleted (10,000 RCF, 10 min), and analyzed (50 μL) by LC-MS/MS as described above. The concentration of CA4 in plasma (ng CA4 / mL) was obtained by multiplying the LC-MS/MS concentration by 2 and the concentration of CA4 in tumors/organs (ng CA4 / g tumor or organ) was obtained by multiplying the LC-MS/MS concentration by 5. Pharmacokinetics were calculated by WinNonlin (Pharsight) using the non-compartmental method. Average radiance was then determined 2, 6, and 24 hr after IV injection by injecting D-Luciferin i.p. and measuring by IVIS. (A) Average percent of injected dose ± SEM (n = 6 mice / time point) was determined from the mass of CA4 / g tissue and compared to CA4P at the same time point by Kruskal-Wallis nonparametric ANOVA with Dunn's post-test. Average issue to plasma ratios ± propagated SEM were calculated from data in A and drug plasma concentrations at the indicated time point from PK data in Table 1 and compared to CA4P at the same time point by one way ANOVA with Tukey's post-test.

RESULTS

Relationship between molar ratio of ethylenediamine to NHS-activated F127 and extent of PEO block cross-linking

The PEO shells of Pluronic F127 polymer micelles (F127 PM) were peripherally cross-linked with ethylenediamine (ED) (Fig.2) by (**i**.) reacting the terminal hydroxyl end-groups of Pluronic F127 unimers (**1**) with DSC to form NHS-activated F127 (NHS-F127) (**2a**) and

(**ii**.) incubating subsequent NHS-activated F127 polymer micelles (NHS- F127 PM) (**2b**) with ethylenediamine (ED) to form shell cross-linked F127 PM (X-F127 PM) (**3**).

To determine the relationship between the molar ratio of ED cross-linker to NHS-F127 PM and the extent of PEO cross-linking under our reaction conditions, we compared the percent of total F127 PM PEO blocks cross-linked with ED at increasing molar ratios of ED/NHS-F127 by ^{1}H-NMR (Fig.S1 & 3). NHS-activated hydroxyls of NHS-F127 PM did not hydrolyze under these reaction conditions (data not shown) as determined by ^{1}H-NMR (Fig.S1A, peak 2/peak 5). Increasing the molar ratio of ED/NHS-F127 over a range of 0.1 to 1 increased the percent of total PEO blocks cross-linked with ED up to 76% in a nonlinear manner [R^2 = 0.9975, n=2 from same batch] (Fig.3) with no detectable levels of monovalent ED conjugation (Fig.S1C). In contrast, molar ratios of ED/NHS-F127 ≥ 2 produced inconsistent levels of ED cross-linking (data not shown) and detectable levels of monovalent ED conjugation (Fig.S1B, peak 4) possibly because DSC-activated OH groups become inaccessible to monovalent ED conjugates at higher levels of divalent ED conjugation. Thus, increasing molar ratios of ED/NHS-F127 to somewhere between 1 and 2 reproducibly increases ED cross-linking of PEO blocks under the current reactions conditions.

Effect of peripheral shell cross-linking on size of F127 PM in solution and lyophilized form

Although the proportion of ED cross-linking between PEO blocks of F127 PM could be determined by ^{1}H-NMR (Figs.3 & S1), it remained unclear whether the peripheral cross-links are within the shells of individual F127 PM (intramicellar) and/or between the shells of multiple F127 PM (intermicellar). It was also possible that intramicellar cross-links with ED compromise the ability of the micelle shell to prevent the aggregation of F127 PM in solution.

To determine if peripheral shell cross-linking with ED is intramicellar and/or intermicellar under the current reaction conditions or causes F127 PM to aggregate in solution, we compared the diameters of F127 PM at increasing levels of ED cross-linking in solution or lyophilized form by DLS and AFM, respectively (Fig.4). Increasing ED cross-linking to a maximum of 76% of total PEO blocks did not change the diameter of F127 PM in PBS [R^2 = 0.03041, P = 0.7411, n = 3 from same batch] (Fig.4A, open squares) or in lyophilized form [R^2 = 0.3861, P = 0.1879, n = 30 micelles] (Fig.4A, closed squares) but steadily increased the height [R^2 = 0.9767, P = 0.0002, n = 30 micelles] (Fig.4B, closed triangles) and height/diameter (H/D) ratio [R^2 = 0.9508, P = 0.0009, n = 30 micelles] of lyophilized X-F127 PM (Fig.4B, closed circles). Furthermore, the polydispersity index of all samples in PBS ranged from 0.112 to 0.178 (data not shown), indicating a narrow size distribution, whereas larger peaks indicative of PM aggregation were not observed. Thus, peripheral shell cross-links with ED up to at least 76% of total PEO blocks are within the shells of individual F127 PM (i.e., intramicellar) under these reaction conditions and increase the rigidity of F127 PM without causing aggregation in solution.

Effect of peripheral shell cross-linking on CA4 loading and aqueous solubility

Combretastatin A4 (CA4) is a low MW drug with poor aqueous solubility (~27 μg CA4/mL) that disrupts the function of established tumor vasculature (35) and shows much promise in

the multi-modality treatment of cancer. The cardiotoxicity of CA4, however, is dose-limiting (35, 36). Thus, CA4 is a good model drug for these studies where decreasing the amount of physically loaded CA4 that is prematurely released after IV administration is likely to increase CA4 localization to the primary tumor and decrease localization to the heart and other peripheral tissues.

To first determine if peripheral shell cross-linking with ED affects physical drug loading in F127 PM by the solid dispersion method, we compared CA4 loading in F127 PM cross-linked with ED at 76% of total PEO blocks (X- F127 PM) to F127 PM at 12.9 wt% and 22.9 wt% CA4 loading by LC-MS/MS (Fig.5A). X-F127 PM increased CA4 loading by 1.5% [12.2 ± 0.6 (SD) vs. 10.7 ± 0.4 CA4 wt%, $P = 0.0255$, n = 3 from same batch] and CA4 encapsulation efficiency by 11.9% [95 ± 2 (SD) vs. 82.9 ± 2%, $P = 0.0251$, n = 3 independent samples from same batch] over F127 PM at 12.9 wt% theoretical CA4 loading (Fig.5A). In contrast, there was no difference in loading or encapsulation efficiency when loading was increased to 22.9 wt% by doubling the amount of CA4 (Fig.5A, ↑**CA4**) or using half the amount of F127 PM (Fig.5A, ↓**F127**) in the solid dispersion. Thus, peripheral shell cross-linking with ED up to at least 76% of total PEO blocks may increase physical drug loading by the solid dispersion method at lower levels of drug loading.

To next determine if peripheral shell cross-linking with ED and/or CA4 loading affects the aqueous solubility of CA4 physically loaded in F127 PM by the solid dispersion method, we compared the aqueous solubility of CA4 loaded in X-F127 PM to CA4 loaded in F127 PM at 12.9 wt% or 22.9 wt% by LC-MS/MS at 10 mg CA4/mL dH_2O theoretical (~370-fold increase in CA4 aqueous solubility) (Fig.5B). Increasing CA4 loading by doubling the amount of CA4 (Fig.5B, ↑**CA4**) or using half the amount of F127 PM (Fig.5B, ↓**F127**) in the solid dispersion did not affect the aqueous solubility of CA4 loaded in F127 PM or X-F127 PM compared to uncross-linked F127 PM at 12.9 wt% ($P \geq 0.3079$) (Fig.5B). Thus, peripheral shell cross-linking with ED up to at least 76% of total PEO blocks is unlikely to affect the aqueous solubility of CA4 loaded in F127 PM up to at least 10 mg CA4/mL regardless of the approach to increase the wt% of CA4 in the solid dispersion up to 22.9 wt % even under suboptimal solubilization conditions.

Effect of peripheral shell cross-linking and CA4 loading on the diameter of F127 PM in human serum

An important role of the polymer micelle shell is to prevent the aggregation of polymer micelles after i.v administration that can decrease the plasma half-life of loaded drug, increase the distribution of loaded drug to the liver, and lead to the formation of pulmonary emboli (5). Although peripheral shell cross-linking with ED up to at least 76% of total PEO blocks does not cause F127 PM to aggregate in PBS (Fig.4A, open squares), it remained possible that it causes aggregation in the presence of proteins encountered after IV administration.

To determine if peripheral shell cross-linking with ED causes F127 PM to aggregate in physiologically relevant concentrations of serum, we compared the diameters of empty and CA4-loaded (22.9 wt%) X-F127 PM with empty and CA4-loaded F127 PM by DLS after incubation at 37°C in buffer or 90% (v/v) human serum for 24 h (Fig.6). There was no

statistical difference between the diameters of X-F127 PM and F127 PM after incubation in PBS (Fig.6, open bars) or 90% (v/v) human serum (Fig.6, closed bars) in the absence or presence of loaded CA4 [$P = 0.1945$]. Furthermore, the polydispersity index of all the samples ranged from 0.143 to 0.269, indicating a narrow size distribution, whereas larger peaks indicative of aggregation were not observed (data not shown). Thus, peripheral shell cross-linking with ED up to at least 76% of total PEO blocks does not cause empty or CA4-loaded F127 PM (22.9 wt%) to aggregate in physiologically relevant concentrations of human serum at 37°C for at least 24 h under static conditions.

Effect of peripheral shell cross-linking on the potency of physically loaded CA4 against HUVEC growth *in vitro*

To determine if high levels of peripheral shell cross-linking with ED affect the release rate of physically loaded drug from F127 PM, we compared the IC_{50} of CA4 in X-F127 PM at 22.9 wt% against HUVEC growth after 24 h to CA4 loaded in uncross-linked F127 PM and CA4 alone solubilized in DMSO (0.25% v/v) by cell counting with trypan blue (Fig.7). X-F127 PM decreased the IC_{50} of CA4 against HUVEC growth ~12-fold vs. CA4 alone [68 ±1 (SE) vs. 809 ± 1 nM CA4] (Fig.7B), whereas F127 PM decreased the IC_{50} of CA4 ~3-fold vs. CA4 alone [259 ±1 (SE) vs. 809 ± 1 nm CA4] (Fig.7B) with no differences in trypan blue exclusion (~95%) compared to untreated HUVEC (data not shown). There was no statistical difference in the concentrations of CA4 in the 1 mg CA4/mL stock solutions of F127 PM-CA4 and X-F127 PM-CA4 [$P = 0.4733$] as determined by LC-MS/MS, indicating that differences in concentration are not responsible for differences in potency (data not shown). Furthermore, DMSO alone (0.25% v/v) and empty F127 PM or X-F127 PM alone at twice the concentration present with 10 μM CA4 [20.8 μg F127 PM or X-F127 PM/mL] did not affect HUVEC cytotoxicity or growth compared to untreated HUVEC for at least 48 h, indicating that any growth inhibition is due to CA4 activity and not DMSO, F127 PM, or X-F127 PM (data not shown). Thus, peripheral shell cross-linking with ED up to at least 76% of total PEO blocks increases the potency of physically loaded CA4 against HUVEC growth *in vitro* compared to CA4 loaded in uncross-linked F127 PM or CA4 alone.

Effect of peripheral shell cross-linking on the amount of physically loaded CA4 delivered to HUVEC *in vitro*

Given that comparable concentrations of empty F127 PM or X-F127 PM did not affect HUVEC growth or cytotoxicity for at least 48 h and CA4 loaded in X-F127 PM was not cytotoxic at 10 μM CA4 (data not shown), we hypothesized that high levels of peripheral shell cross-linking with ED increase the potency of loaded CA4 by increasing the amount of CA4 delivered to HUVEC during the 4 h treatment window. One potential approach to indirectly monitor the amount of CA4 delivered to HUVEC is with electric cell-substrate impedance sensing (ECIS). ECIS monitors a current that is passed through the growth media via gold electrodes on the surface of a specialized cell culture well (37). Cells that cover the electrodes act as insulators and increase the resistance of the well. As such, changes in the density (38, 39) and/or morphology (40) of cells after treatment with drugs such as CA4 (41, 42) can be indirectly monitored in real-time as time-dependent changes in the resistance of the well relative to untreated cells (43).

To first determine if ECIS is suitable to monitor the activity of CA4 against proliferating HUVEC, we treated HUVEC in the same manner as the IC_{50} studies (Fig.7) and compared increasing concentrations of CA4 in DMSO (0.25% v/v) on the well resistance of proliferating HUVEC to media/DMSO or media alone by ECIS (Fig.8). Treatment with media (Fig.8, Media) or media/DMSO (Fig.8, DMSO 0.25%) alone had similar effects on the resistance of proliferating HUVEC during treatment (Fig.8, "Rx"), whereas media/DMSO slightly decreased the magnitude of post-treatment resistance. In contrast, CA4 in DMSO (Fig.8, DMSO/CA4) decreased the magnitude of HUVEC resistance below media and media/DMSO during and after treatment in a concentration-dependent manner. Thus, ECIS is suitable to indirectly monitor CA4 activity against proliferating HUVEC.

To next indirectly determine if peripheral shell cross-linking with ED increases the amount of CA4 delivered to HUVEC by F127 PM, we compared treatment with CA4 loaded in X-F127 PM at 22.9 wt% on the resistance of proliferating HUVEC to CA4 loaded in uncross-linked F127 PM at 22.9 wt%, CA4 in DMSO, and empty X-F127 PM or empty F127 PM by ECIS (Fig.8). Empty X-F127 PM and empty F127 PM at a concentration present with 100 nM CA4 at 22.9 wt% CA4 (0.1 μg/mL) had a similar effect on the resistance as media alone (Fig.8, Media). In contrast, 100 nM CA4 loaded in X-F127 PM [76%] (Fig.8, X-F127 PM-CA4 100 nM) decreased the resistance of HUVEC to levels similar to 500 nM CA4 in DMSO (Fig.8, DMSO/CA4 500 nM) and 100 nM CA4 in F127 PM (Fig.8, F127 PM-CA4 100 nM) during the treatment window (Fig.8, "Rx") but decreased post-treatment resistance below all the treatment groups. Thus, given that the resistance of proliferating HUVEC is unaffected by empty F127 PM or X-F127 PM and decreases with an increase in CA4 concentration, these results indicate that high levels of peripheral shell cross-linking with ED increase the amount of physically loaded CA4 delivered to proliferating HUVEC.

Effect of peripheral shell cross-linking on the unbound fraction of physically loaded CA4 in human blood

An indirect approach to determine if peripheral shell cross-linking decreases premature release of physically loaded drug from F127 PM in whole blood is to compare the unbound fraction (*fu*) of loaded drug with unencapsulated drug by the erythrocyte vs. buffer or plasma partitioning method (32). A decrease in the *fu* of loaded drug vs. unencapsulated drug indicates that a higher proportion of drug remains within the polymer micelles because completely released drug will have the same *fu* as unencapsulated drug. Furthermore, decreasing the *fu* of the hydrophobic drug cyclosporine A (CyA) in whole blood after loading in core-shell polymer micelles composed of poly(ethylene oxide)-block-poly(ε-caprolactone) copolymers correlates with an increase in bioavailability after IV administration in rats (32) and may predict if a polymer micelle and/or modification such as shell cross-linking is likely to increase the bioavailability of loaded drug after IV administration.

To indirectly determine if high levels of peripheral shell cross-linking are likely to decrease premature release of physically loaded drug from F127 PM after IV administration, we compared the unbound drug fraction (*fu*) of CA4 loaded in X-F127 PM at 22.9 wt% to CA4 loaded in uncross-linked F127 PM and CA4 alone in human whole blood at 37°C by an

erythrocyte vs. buffer or plasma partitioning method (32) at concentrations below the CMC of F127 at 37°C (Fig.9). X-F127 PM decreased the *fu* of CA4 ~16% compared to unencapsulated CA4 [9.7 ± 0.9 (SD) vs. 25.5 ± 0.9% Free CA4, P <0.001], whereas F127 PM decreased the *fu* of CA4 ~7% compared to unencapsulated C4 [18.8 ± 0.6 (SD) vs. 25.5 ± 0.9% Free CA4, P = 0.0002] (Fig.9).Thus, high levels of peripheral shell cross-linking with ED decrease the premature release of physically loaded drug from core-shell polymer micelles in whole blood and are, consequently, likely to increase bioavailability and subsequent potency after IV administration.

Effect of peripheral shell cross-linking on the potency, pharmacokinetics, and distribution of physically loaded CA4 after IV administration in tumor-bearing mice

To determine if high levels of peripheral shell cross-linking increase the potency of physically loaded CA4 in primary breast tumors after IV administration, we compared the extent that CA4 in X-F127 PM (22.9 wt%) affect the vascular function and subsequent growth of primary murine breast tumors that stably express luciferase (4T1-Luc) to CA4 in F127 PM (22.9 wt%), water-soluble CA4 phosphate (CA4P) (42), or PBS by an IVIS-based assay (33) and monitoring tumor volumes, respectively (Fig.10). X-F127 PM increased vascular shutdown by CA4 58% over PBS after 2 hours [68 ± 1 (SD) vs. 10 ± 2%, P < 0.0001], whereas F127 PM increased shutdown by only 10% over PBS [20 ± 2 (SD) vs. 10 ± 2%, P = 0.007], and CA4P had no effect [20 ± 2 (SD) vs. 10 ± 2%, P = 0.5901] (Fig.10A, open bars). Unlike F127 PM, X-F127 PM also maintained vascular shutdown by CA4 over PBS for at least 24 hours (Fig.10A). Furthermore, X-F127 PM (Fig.10B, cross-hatched symbols) increased tumor growth inhibition by CA4 over PBS (Fig.10B, open circles) by Day 5 post-injection [471 ± 54 (SEM) vs. 926 ± 90 mm^3, P = 0.0018], whereas CA4 in F127 PM (Fig.10B, closed squares) and CA4P (Fig.10B, closed circles) had no effect [710 ± 71 (SEM) and 792 ± 86 mm^3 vs. 926 ± 90 mm^3, P = 0.2779 & P > 0.9999]. Thus, high levels of peripheral shell cross-linking with ED up to at least 76% of total PEO blocks increase the potency of physically loaded CA4 in primary breast tumors after IV administration.

To determine if high levels of peripheral shell cross-linking increase the potency of physically loaded CA4 in primary breast tumors by affecting the pharmacokinetics of CA4, we compared the pharmacokinetic parameters of CA4 loaded in X-F127 PM (22.9 wt%) to CA4 loaded in F127 PM (22.9 wt%) or water-soluble CA4 phosphate (CA4P) over 24 hours after IV administration in 4T1-Luc tumor-bearing mice by LC-MS/MS at the same dose as Fig.10 (Table 1, Fig.S2, Table S2). AUC_{last} was similar to $AUC_{0-\infty}$ for each treatment group, indicating that the selected time points adequately covered the respective PK profiles (Table 1, AUC_{last} and $AUC_{0-\infty}$). Although X-F127 PM decreased the *fu* of CA4 below F127 PM (Fig.9) and was, consequently, expected to increase bioavailability over F127 PM after IV administration (32), both X-F127 PM and F127 PM increased the bioavailability of CA4 ~1.5-fold over CA4P. In contrast, X-F127 PM increased the mean residence time of CA4 ~2-fold over CA4 in F127 PM and ~5-fold over CA4P and increased the plasma half-life of CA4 1.25-fold over CA4 loaded in F127 PM and ~3-fold over water-soluble CA4P (Table 1, $MRT_{0-\infty}$ & $t_{0.5}$). Furthermore, X-F127 PM increased the volume of distribution of CA4 ~2-fold over CA4 in F127 PM and ~3-fold over CA4P (Table 1, V_{ss}) and both X-F127 PM and

F127 PM decreased the clearance rate of physically loaded CA4 ~1.5-fold compared to water-soluble CA4P (Table 1, CL). Thus, high levels of peripheral shell cross-linking increase the potency of physically loaded CA4 against primary breast tumors after IV administration, in part, by increasing the mean residence time of CA4.

To determine if high levels of peripheral shell cross-linking increase the potency of physically loaded CA4 in primary breast tumors by affecting the distribution of CA4, we compared the distribution and tissue/plasma ratio of CA4 loaded in X-F127 PM (22.9 wt%) to CA4 loaded in F127 PM (22.9 wt%) or CA4P 2 and 24 hours after IV administration in 4T1-Luc tumor-bearing mice by LC-MS/MS at the same dose used in Fig.10 (Fig. 11 & Table S3). X-F127 PM (Fig.11A, closed bars) increased the percent of injected dose (%ID) in primary 4T1-Luc tumors ~20% over CA4P (Fig.11A, open bars) after 2 hours [21 ± 6 (SEM) vs. 0.6 ± 0.1%, $P = 0.0045$] but not 24 hours [5 ± 3 (SEM) vs. 0.04 ± 0.04%, $P = 0.0866$], whereas F127 PM (Fig.11A, grey bars) increased the %ID ~12% over CA4P after 2 hours [13 ± 2 (SEM) vs. 0.6 ± 0.1%, $P = 0.0243$] and 24 hours [13 ± 2 (SEM) vs. 0.04 ± 0.04%, $P = 0.0031$]. There was, however, no statistical difference between X-F127 PM and F127 PM after 2 [$P > 0.9999$] or 24 hours [$P > 0.5272$]. Furthermore, X-F127 PM did not statistically increase the tissue/plasma (T/P) ratio of CA4 in 4T1-Luc tumors (Fig.11B, closed bars) over CA4P (Fig.11B, open bars) after 2 hours [109 ± 52 (SEM) vs. 3 ± 2, $P = 0.1242$] or 24 hours [99 ± 62 (SEM) vs. 10 ± 7, $P = 0.8514$], whereas F127 PM (Fig.11B, grey bars) statistically increased the T/P ratio of CA4 50-fold over CA4P after 2 hours [140 ± 42 (SEM) vs. 3 ± 2, $P = 0.0435$] but not 24 hours [402 ± 221 (SEM) vs. 10 ± 7, $P = 0.0957$]. Both X-F127 PM and F127 PM eventually decreased the %ID and T/P ratio of CA4 in the heart and kidneys significantly below CA4P but, with the exception of F127 PM in the liver after 2 hours, the %ID and T/P ratios of CA4 in the liver, lungs, and spleen were statistically similar to CA4P (Fig.11). Thus, both X-F127 PM and F127 PM increase the distribution of physically loaded CA4 to primary murine breast tumors of 4T1-Luc and greatly decrease distribution to the heart and kidneys compared to CA4P but statistical differences between X-F127 PM or F127 PM were not observed after 2 or 24 hours under the current experimental conditions.

DISCUSSION

This study provides evidence that peripherally cross-linking the shell of core-shell polymer micelles at high levels increases the potency of physically loaded drugs against primary murine breast tumors after IV administration. We found that peripherally cross-linking the shell of F127 PM with ethylenediamine (ED) at 76% of the total PEO blocks increased the potency of physically loaded CA4 against the vascular function and subsequent growth of 4T1-Luc tumors over CA4 loaded in F127 PM and water-soluble CA4P (Fig.10). Furthermore, this study shows that high levels of peripheral shell cross-linking are unlikely to interfere with the ability of core-shell polymer micelles to function as drug nanocarriers. We found that peripherally cross-linking the shell of F127 PM at 76% (i.) does not affect CA4 loading by the solid dispersion method to at least 22.9 wt% (Fig.5A), (ii.) does not affect the aqueous solubility of loaded CA4 to at least 10 mg CA4/mL (Fig.5B), (iii.) does not cause CA4-loaded F127 PM to aggregate in buffer or 90% (v/v) human serum at 37°C for at least 24 h (Fig.6), and (iv.) does not affect the release rate of loaded drug as shown by

an increase in the potency of loaded CA4 against HUVEC growth *in vitro* compared to CA4 loaded in F127 PM or solubilized in water with DMSO (Fig.7).

Effect of peripheral shell cross-linking F127 PM on the potency of loaded CA4 after IV administration

There are at least two possible reasons that may singly or collectively explain why high levels of peripheral shell cross-linking increase the potency of physically loaded CA4 against primary murine breast tumors. The first possible reason that high levels of peripheral cross-linking increase the potency of physically loaded CA4 is by increasing the rate and extent that CA4 accumulates in primary tumors through a decrease in the premature release of CA4 from F127 PM after IV administration and, consequently, delivering more CA4 per PM relative to uncross-linked F127 PM. This is supported by our findings that X-F127 PM (i.) decreased the unbound drug fraction of physically loaded CA4 in whole blood (*fu*) compared to F127 PM and unencapsulated CA4 (Fig.9) where a decrease in the *fu* indicates a decrease in drug release (32), (ii.) increased the mean residence time of CA4 after IV administration over CA4 in F127 PM (Table 1), and (iii.) increased the extent and duration of vascular shutdown over CA4 in F127 PM (Fig.10). Although there was no statistical difference between the %ID and T/P ratios of CA4 in primary tumors by X-F127 PM and F127 PM after 2 hours (Fig.11), X-F127 PM increased vascular shutdown over F127 PM for at least 24 hours (Fig.10) and is, consequently, expected to decrease the subsequent passive accumulation of nanocarriers in primary tumors (19) to a greater extent. Thus, it is likely that statistical differences between the %ID and T/P ratios of X-F127 PM and F127 PM in primary tumors occur at time points earlier than 2 hours.

The second possible reason that high levels of peripheral shell cross-linking increase the potency of physically loaded CA4 against primary murine breast tumors is by increasing the affinity of F127 PM for the surface of vascular endothelial cells within tumor vasculature and, consequently, increasing the total number of CA4-loaded PM that are internalized. This is supported by our findings that X-F127 PM increased the potency (Fig.7) and extent (Fig. 8) of CA4 that is delivered to HUVEC over CA4 loaded in F127 PM and that HUVEC growth and resistance was unaffected by empty F127 PM or X-F127 PM. It remains possible, however, that the increase in the potency and extent of CA4 delivery to HUVEC by X-F127 PM is instead due to a decrease in the amount of physically loaded CA4 that is potentially released by 10% FBS within the HUVEC media. This would remain consistent with our finding that X-F127 PM decreased the unbound drug fraction (*fu*) of CA4 in whole blood compared to uncross-linked F127 PM (Fig.9).

Effect of peripheral shell cross-linking F127 PM on the premature release of loaded CA4 in serum and whole blood

There are at least three possible reasons that may singly or collectively explain why high levels of peripheral shell cross-linking decrease the premature release of loaded CA4 from F127 PM in whole blood. The first possible reason is that high levels of peripheral shell cross-linking decrease premature release of loaded CA4 in whole blood by increasing the crystallinity of loaded CA4 (44) and, consequently, block or slow the rate that CA4 is accessible to drug binding components in the blood. This is unlikely, however, given that the

half-widths of the Tm peaks for CA4 loaded in X-F127 PM, CA4 loaded in F127 PM, and unencapsulated CA4 determined by DSC were similar (data not shown), indicating that high levels of peripheral shell cross-linking do not affect the crystallinity of loaded CA4.

The second possible reason is that high levels of peripheral shell cross-linking decrease premature release of loaded CA4 in whole blood by preventing the disassembly of F127 PM and, consequently, minimizing the exposure of loaded drug to drug binding components in the blood (22, 24). This remains possible given that the concentration of uncross-linked F127 PM used to determine the *fu* of loaded CA4 in this study (0.057 mg F127 / mL) was less than the CMC of F127 at 37°C (~0.189 mg F127 / mL (45)). Uncross-linked F127 PM, however, also decreased the *fu* of CA4 below unencapsulated CA4 (i.e., also decreased premature drug release, albeit to a lesser extent than X-F127 PM), suggesting that disassembly does not occur or takes longer than the 2 hour time point. Furthermore, the presence of loaded drug alone can decrease both the CMC and rate of PM disassembly (5). Thus, it remains unclear whether peripheral shell cross-linking decreases premature drug release in whole blood by preventing the disassembly of F127 PM.

The third possible reason is that high levels of peripheral shell cross-linking decrease premature release of loaded CA4 in whole blood by minimizing or blocking interactions between the PEO shells of intact F127 PM and proteins/lipid bilayers within the blood that lead to close contact between the drug-loaded hydrophobic core and lipid membranes (46). Peripheral shell cross-linking then, consequently, blocks, minimizes, or slows the membrane-mediated transfer of physically loaded hydrophobic drug from the core of core-shell PM to the lipid membranes of erythrocytes and/or WBCs within the blood (47). This is supported by our finding that X-F127 PM decreased the unbound drug fraction of physically loaded CA4 in whole blood (*fu*) compared to F127 PM and unencapsulated CA4 (Fig.9) where a decrease in the *fu* indicates a decrease in drug release (32). Peripheral shell cross-linking may also have similar effects on the possible transfer of loaded hydrophobic drug from intact core-shell PM to albumin and α-glycoprotein, proteins that are largely responsible for drug binding in the plasma (47).

CONCLUSIONS

In summary, our results indicate that peripherally cross-linking the shell of core-shell polymer micelles at high levels increases the potency of physically loaded hydrophobic drug against primary murine breast tumors after IV administration, in part, by decreasing premature drug release in the blood and, consequently, increasing the mean residence time of physically loaded hydrophobic drug in plasma without compromising the ability of F127 PM to function as drug nanocarriers. Thus, peripherally cross-linking the shells of core-shell polymer micelles may be a simple approach to decrease the premature release of physically loaded hydrophobic drugs in the blood and increase subsequent potency in solid tumors after IV administration.

Supplementary Material

Refer to Web version on PubMed Central for supplementary material.

ACKNOWLEDGEMENTS

This work was supported by NIH COBRE grant 2P20GM103480-06 (Nebraska Center for Nanomedicine) (RRW, RKS, JAV), NIH 1U54CA163120-01 grant (RKS), and UNMC Predoctoral Fellowships (SPRB, ST, VVA). The Nanoimaging Core Facility was supported by the NIH (SIG program), the UNMC Program of Excellence (POE), and the Nebraska Research Initiative (NRI). The Authors would also like to acknowledge Todd A. Wyatt, PhD and the VA Nebraska-Western Iowa Health Care System Research Service for providing access to and assistance with the Electric Cell Impedance Sensing apparatus.

ABBREVIATIONS

4T1	Syngeneic murine breast tumor epithelial cells
4T1-Luc	4T1 cells that stably express luciferase
AFM	Atomic force microscopy
CA4	Combretastatin A4
CA4P	Combretastatin A4 Phosphate / Fosbretabulin disodium
DLS	Dynamic light scattering
DMSO	Dimethyl sulfoxide
DSC	N,N’-Disuccinimidyl carbonate
ECIS	Electric cell-substrate impedance sensing
ED	Ethylenediamine
F127	Pluronic F127 (Poloxamer 407)
F127 PM	Pluronic F127 polymer micelles
fu	Unbound fraction of drug in whole blood
HUVEC	Human umbilical vein endothelial cells
IVIS	*In vivo* imaging system
NHS-F127	DSC-activated Pluronic F127
NHS-F127 PM	DSC-activated Pluronic F127 polymer micelles
X-F127 PM	Pluronic F127 polymer micelle shell cross-linked with ED at 76%;

REFERENCES

1. Allen, LV.; Popovich, NG.; Ansel, HC. Ansel’s pharmaceutical dosage forms and drug delivery systems. Philadelphia: Wolters Kluwer Health/Lippincott Williams & Wilkins; 2011. Parenterals; p. 432-433.
2. Williams HD, Trevaskis NL, Charman SA, Shanker RM, Charman WN, Pouton CW, Porter CJ. Strategies to address low drug solubility in discovery and development. Pharmacological reviews. 2013; 65(1):315–499. [PubMed: 23383426]
3. Teicher, BA. Anticancer Drug Development Guide: Preclinical Screening, Clinical Trials, and Approval. Humana Press; 1997.
4. Yalkowsky SH. Techniques of Solubilization of Drugs: Books on Demand. 1993

5. Batrakova, EV.; Bronich, TK.; Vetro, JA.; Kabanov, AV. Polymeric Micelles as Drug Carriers. In: Torchilin, VP., editor. Nanoparticulates as Drug Carriers. London: Imperial College Press; 2006. p. 57-93.

6. Torchilin VP. Structure and design of polymeric surfactant-based drug delivery systems. Journal of controlled release : official journal of the Controlled Release Society. 2001; 73(2–3):137–172. [PubMed: 11516494]

7. Kataoka K, Harada A, Nagasaki Y. Block copolymer micelles for drug delivery: design, characterization and biological significance. Adv Drug Deliv Rev. 2001; 47(1):113–131. [PubMed: 11251249]

8. Kabanov AV, Alakhov VY. Pluronic block copolymers in drug delivery: from micellar nanocontainers to biological response modifiers. Crit Rev Ther Drug Carrier Syst. 2002; 19(1):1–72. [PubMed: 12046891]

9. Adams ML, Lavasanifar A, Kwon GS. Amphiphilic block copolymers for drug delivery. J Pharm Sci. 2003; 92(7):1343–1355. [PubMed: 12820139]

10. Duncan R. The dawning era of polymer therapeutics. Nat Rev Drug Discov. 2003; 2(5):347–360. [PubMed: 12750738]

11. Bulmus V, Woodward M, Lin L, Murthy N, Stayton P, Hoffman A. A new pH-responsive and glutathione-reactive, endosomal membrane-disruptive polymeric carrier for intracellular delivery of biomolecular drugs. J Control Release. 2003; 93(2):105–120. [PubMed: 14636717]

12. Veronese FM, Morpurgo M. Bioconjugation in pharmaceutical chemistry. Farmaco. 1999; 54(8): 497–516. [PubMed: 10510847]

13. D'Souza AJ, Topp EM. Release from polymeric prodrugs: linkages and their degradation. Journal of pharmaceutical sciences. 2004; 93(8):1962–1979. [PubMed: 15236447]

14. Bae Y, Fukushima S, Harada A, Kataoka K. Design of environment-sensitive supramolecular assemblies for intracellular drug delivery: Polymeric micelles that are responsive to intracellular pH change. Angewandte Chemie, International Edition. 2003; 42(38):4640–4643. S4640/4641-S4640/4611.

15. Torchilin VP. Micellar nanocarriers: pharmaceutical perspectives. Pharmaceutical research. 2007; 24(1):1–16. [PubMed: 17109211]

16. Hurter PN, Hatton TA. Solubilization of polycyclic aromatic hydrocarbons by poly(ethylene oxide-propylene oxide) block copolymer micelles: effects of polymer structure. Langmuir. 1992; 8(5): 1291–1299.

17. Nagarajan R, Ganesh K. Comparison of solubilization of hydrocarbons in (PEO-PPO) diblock versus (PEO-PPO-PEO) triblock copolymer micelles. J Colloid Interface Sci. 1996; 184(2):489–499. [PubMed: 8978552]

18. Xing L, Mattice WL. Strong solubilization of small molecules by triblock-copolymer micelles in selective solvents. Macromolecules. 1997; 30(6):1711–1717.

19. Matsumura Y, Maeda H. A new concept for macromolecular therapeutics in cancer chemotherapy: mechanism of tumoritropic accumulation of proteins and the antitumor agent smancs. Cancer research. 1986; 46(12 Pt 1):6387–6392. [PubMed: 2946403]

20. Danson S, Ferry D, Alakhov V, Margison J, Kerr D, Jowle D, Brampton M, Halbert G, Ranson M. Phase I dose escalation and pharmacokinetic study of pluronic polymer-bound doxorubicin (SP1049C) in patients with advanced cancer. Br J Cancer. 2004; 90(11):2085–2091. [PubMed: 15150584]

21. Gabizon A, Catane R, Uziely B, Kaufman B, Safra T, Cohen R, Martin F, Huang A, Barenholz Y. Prolonged circulation time and enhanced accumulation in malignant exudates of doxorubicin encapsulated in polyethylene-glycol coated liposomes. Cancer research. 1994; 54(4):987–992. [PubMed: 8313389]

22. Savic R, Eisenberg A, Maysinger D. Block copolymer micelles as delivery vehicles of hydrophobic drugs: micelle-cell interactions. Journal of drug targeting. 2006; 14(6):343–355. [PubMed: 17092835]

23. Matsumura Y, Hamaguchi T, Ura T, Muro K, Yamada Y, Shimada Y, Shirao K, Okusaka T, Ueno H, Ikeda M, Watanabe N. Phase I clinical trial and pharmacokinetic evaluation of NK911, a micelle-encapsulated doxorubicin. Br J Cancer. 2004; 91(10):1775–1781. [PubMed: 15477860]

24. van NCF. Covalently cross-linked amphiphilic block copolymer micelles. Soft Matter. 2011; 7(7): 3246–3259.
25. Thurmond KB II, Kowalewski T, Wooley KL. Water-Soluble Knedel-like Structures: The Preparation of Shell-Cross-Linked Small Particles. J Am Chem Soc. 1996; 118(30):7239–7240.
26. O'Reilly RK, Hawker CJ, Wooley KL. Cross-linked block copolymer micelles: functional nanostructures of great potential and versatility. Chemical Society reviews. 2006; 35(11):1068–1083. [PubMed: 17057836]
27. Read ES, Armes SP. Recent advances in shell cross-linked micelles. Chem Commun (Cambridge, U K). 2007; (29):3021–3035.
28. Li Y, Xiao K, Luo J, Xiao W, Lee JS, Gonik AM, Kato J, Dong TA, Lam KS. Well-defined, reversible disulfide cross-linked micelles for on-demand paclitaxel delivery. Biomaterials. 2011; 32(27):6633–6645. [PubMed: 21658763]
29. Lee S-Y, Kim S, Tyler JY, Park K, Cheng J-X. Blood-stable, tumor-adaptable disulfide bonded mPEG-(Cys)4-PDLLA micelles for chemotherapy. Biomaterials. 2013; 34(2):552–561. [PubMed: 23079665]
30. Koo AN, Min KH, Lee HJ, Lee SU, Kim K, Kwon IC, Cho SH, Jeong SY, Lee SC. Tumor accumulation and antitumor efficacy of docetaxel-loaded core-shell-corona micelles with shell-specific redox-responsive cross-links. Biomaterials. 2012; 33(5):1489–1499. [PubMed: 22130564]
31. Kwon SH, Kim SY, Ha KW, Kang MJ, Huh JS, Im TJ, Kim YM, Park YM, Kang KH, Lee S, Chang JY, Lee J, Choi YW. Pharmaceutical evaluation of genistein-loaded pluronic micelles for oral delivery. Archives of pharmacal research. 2007; 30(9):1138–1143. [PubMed: 17958332]
32. Aliabadi HM, Brocks DR, Mahdipoor P, Lavasanifar A. A novel use of an in vitro method to predict the in vivo stability of block copolymer based nano-containers. Journal of controlled release : official journal of the Controlled Release Society. 2007; 122(1):63–70. [PubMed: 17644207]
33. Zhao D, Richer E, Antich PP, Mason RP. Antivascular effects of combretastatin A4 phosphate in breast cancer xenograft assessed using dynamic bioluminescence imaging and confirmed by MRI. FASEB J. 2008; 22(7):2445–2451. [PubMed: 18263704]
34. Ambardekar VV, Wakaskar RR, Sharma B, Bowman J, Vayaboury W, Singh RK, Vetro JA. The efficacy of nuclease-resistant Chol-siRNA in primary breast tumors following complexation with PLL-PEG(5K). Biomaterials. 2013; 34(20):4839–4848. [PubMed: 23557861]
35. Cooney MM, van Heeckeren W, Bhakta S, Ortiz J, Remick SC. Drug insight: vascular disrupting agents and angiogenesis--novel approaches for drug delivery. Nat Clin Pract Oncol. 2006; 3(12): 682–692. [PubMed: 17139319]
36. Horsman MR, Siemann DW. Pathophysiologic effects of vascular-targeting agents and the implications for combination with conventional therapies. Cancer research. 2006; 66(24):11520–11539. [PubMed: 17178843]
37. Giaever I, Keese CR. Monitoring fibroblast behavior in tissue culture with an applied electric field. Proceedings of the National Academy of Sciences of the United States of America. 1984; 81(12): 3761–3764. [PubMed: 6587391]
38. Lundien MC, Mohammed KA, Nasreen N, Tepper RS, Hardwick JA, Sanders KL, Van Horn RD, Antony VB. Induction of MCP-1 expression in airway epithelial cells: role of CCR2 receptor in airway epithelial injury. Journal of clinical immunology. 2002; 22(3):144–152. [PubMed: 12078856]
39. Zudaire E, Cuesta N, Murty V, Woodson K, Adams L, Gonzalez N, Martinez A, Narayan G, Kirsch I, Franklin W, Hirsch F, Birrer M, Cuttitta F. The aryl hydrocarbon receptor repressor is a putative tumor suppressor gene in multiple human cancers. J Clin Invest. 2008; 118(2):640–650. [PubMed: 18172554]
40. Tiruppathi C, Malik AB, Del Vecchio PJ, Keese CR, Giaever I. Electrical method for detection of endothelial cell shape change in real time: assessment of endothelial barrier function. Proceedings of the National Academy of Sciences of the United States of America. 1992; 89(17):7919–7923. [PubMed: 1518814]

41. Grosios K, Holwell SE, McGown AT, Pettit GR, Bibby MC. In vivo and in vitro evaluation of combretastatin A-4 and its sodium phosphate prodrug. Br J Cancer. 1999; 81(8):1318–1327. [PubMed: 10604728]

42. Galbraith SM, Chaplin DJ, Lee F, Stratford MR, Locke RJ, Vojnovic B, Tozer GM. Effects of combretastatin A4 phosphate on endothelial cell morphology in vitro and relationship to tumour vascular targeting activity in vivo. Anticancer Res. 2001; 21(1A):93–102. [PubMed: 11299795]

43. Hug TS. Biophysical methods for monitoring cell-substrate interactions in drug discovery. Assay and drug development technologies. 2003; 1(3):479–488. [PubMed: 15090185]

44. Ryu J, Jeong YI, Kim IS, Lee JH, Nah JW, Kim SH. Clonazepam release from core-shell type nanoparticles of poly(epsilon-caprolactone)/poly(ethylene glycol)/poly(epsilon-caprolactone) triblock copolymers. Int J Pharm. 2000; 200(2):231–242. [PubMed: 10867253]

45. Alexandridis P, Holzwarth JF, Hatton TA. Micellization of Poly(ethylene oxide)-Poly(propylene oxide)-Poly(ethylene oxide) Triblock Copolymers in Aqueous Solutions: Thermodynamics of Copolymer Association. Macromolecules. 1994; 27(9):2414–2425.

46. Chen H, Kim S, Li L, Wang S, Park K, Cheng JX. Release of hydrophobic molecules from polymer micelles into cell membranes revealed by Forster resonance energy transfer imaging. Proceedings of the National Academy of Sciences of the United States of America. 2008; 105(18): 6596–6601. [PubMed: 18445654]

47. Hinderling PH. Red blood cells: a neglected compartment in pharmacokinetics and pharmacodynamics. Pharmacological reviews. 1997; 49(3):279–295. [PubMed: 9311024]

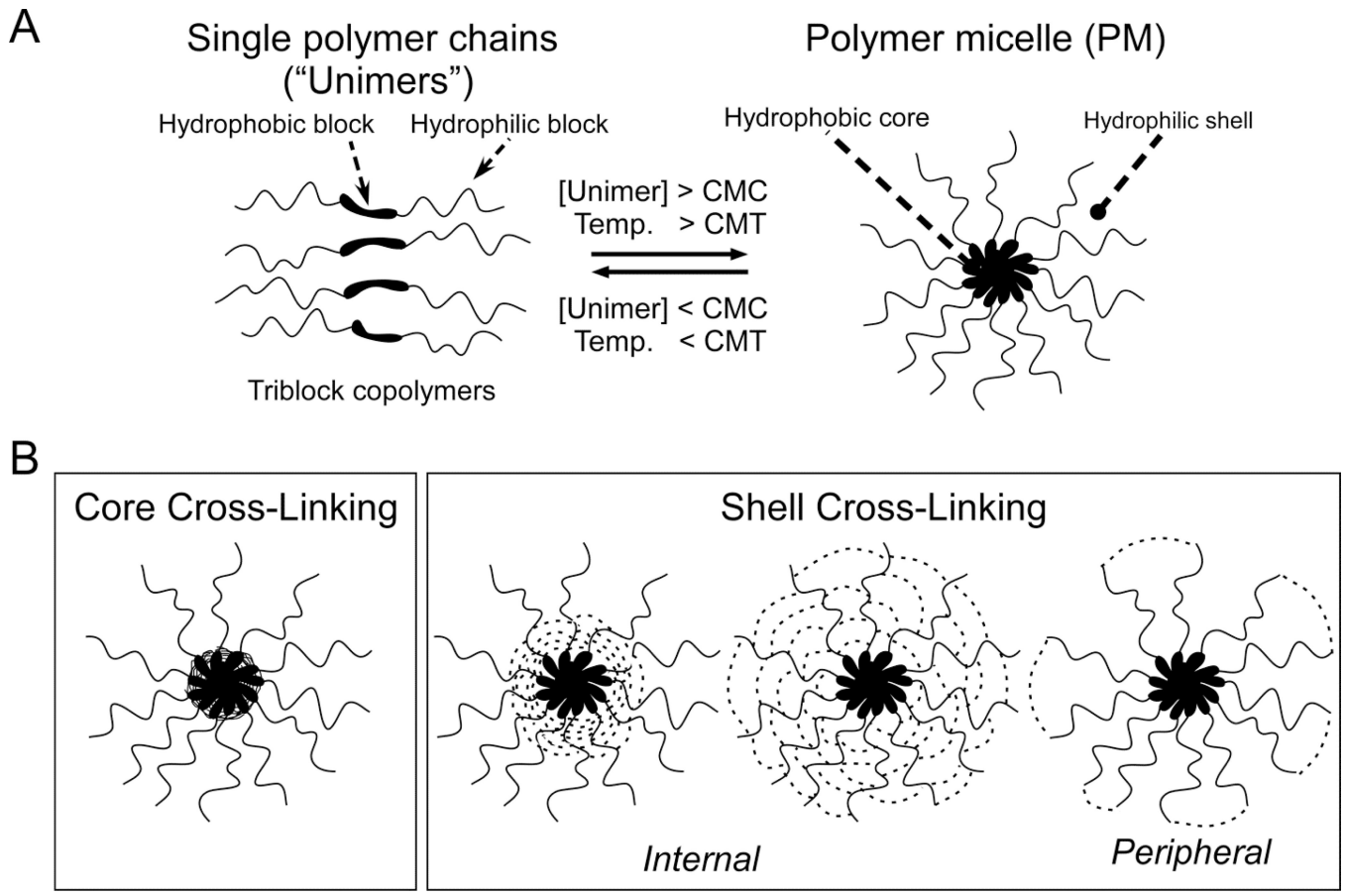

Fig.1.

(A) Self-assembly of polymer micelles from amphiphilic block copolymers. (B) Two major approaches to cross-linking core-shell polymer micelles.

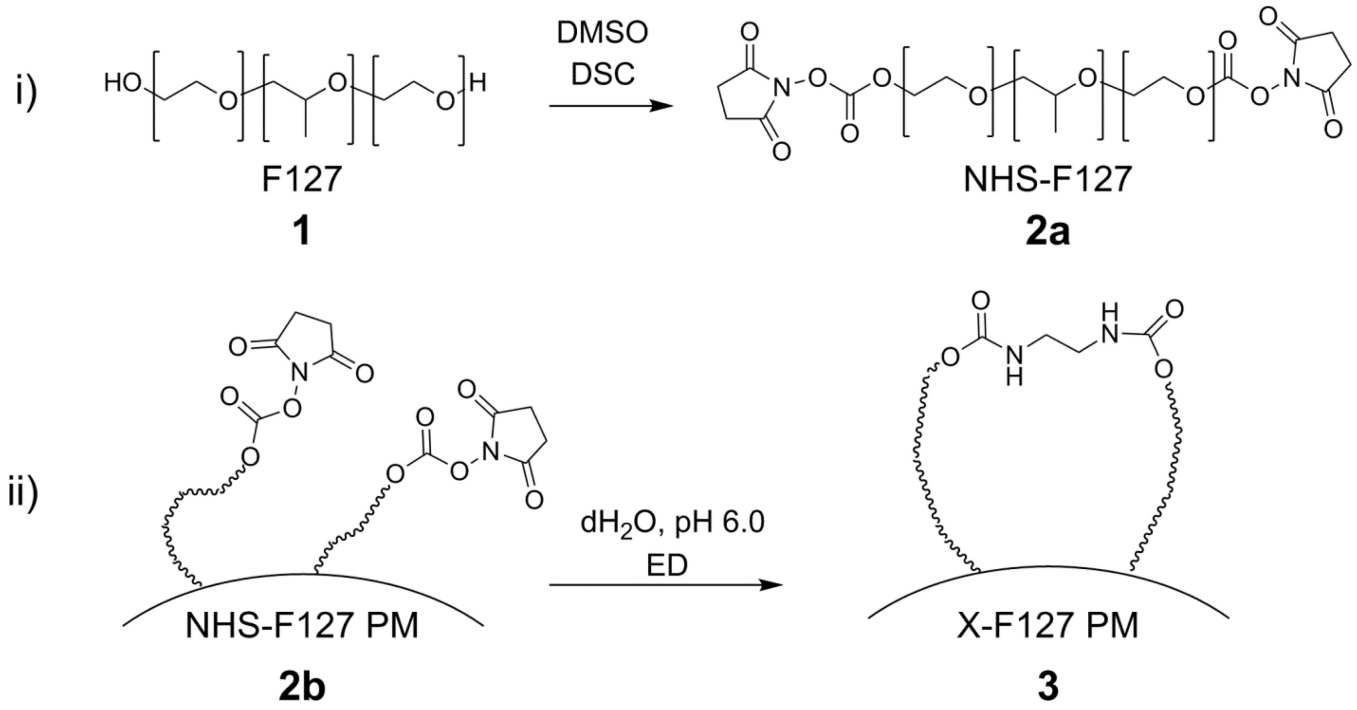

Fig.2.

Synthetic strategy for cross-linking F127 polymer micelle shells with ethylenediamine (ED). The terminal hydroxyl groups of Pluronic F127 (F127) (**1**) were activated with DSC (N,N'-disuccinimidyl carbonate) to form NHS-activated F127 (NHS-F127) (**2a**). Polymer micelles of NHS-F127 (NHS-F127 PM) (**2b**) were then reacted with ED (ethylenediamine) to form shell cross-linked F127 polymer micelles (X-F127 PM) (**3**).

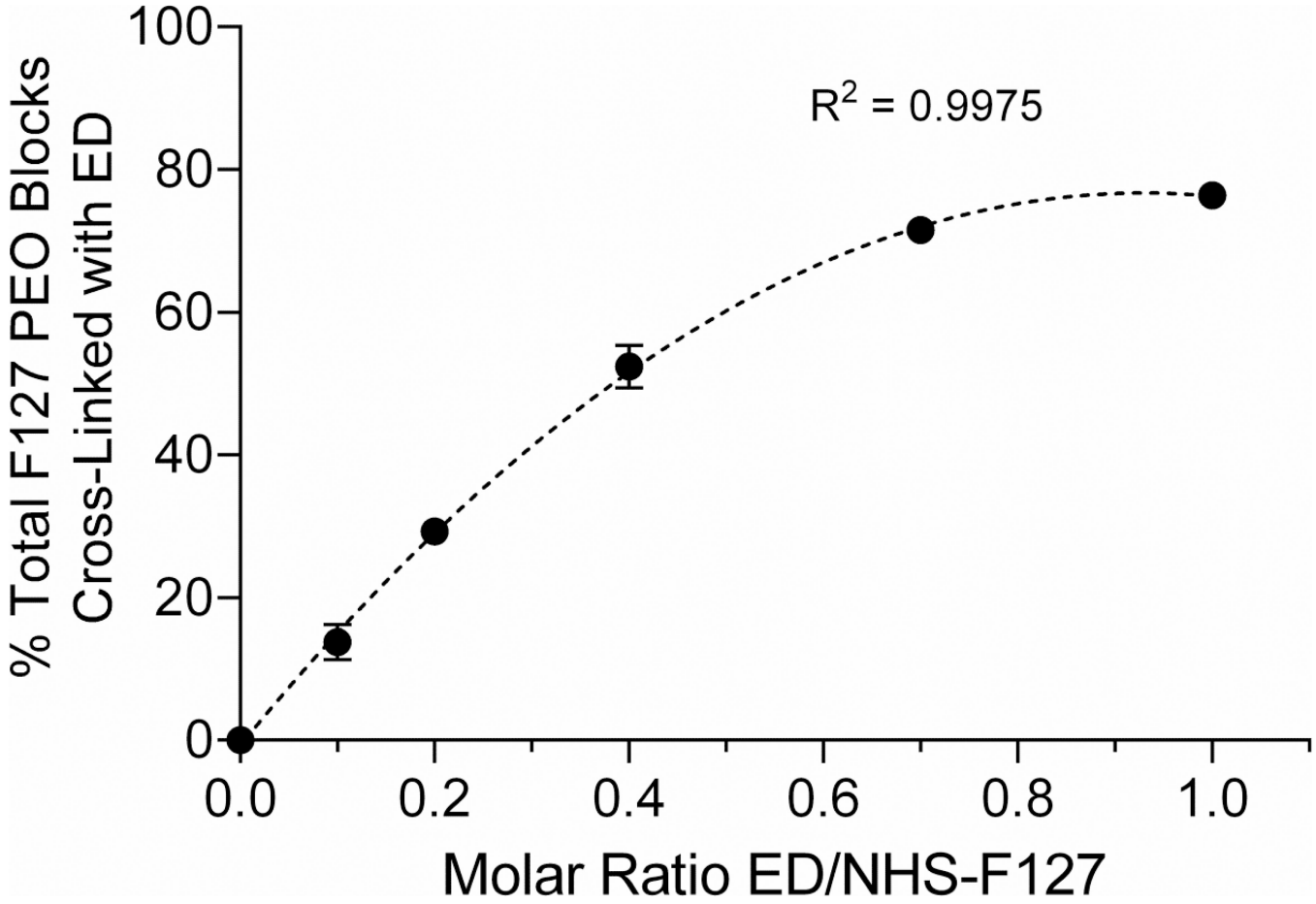

Fig.3.

Relationship between the molar ratio of ethylenediamine (ED) to NHS-activated F127 polymer micelles and the extent that F127 polyethylene oxide blocks (PEO) are cross-linked with ED. Polymer micelles of NHS-activated F127 were incubated with the indicated molar ratio of ED/NHS-F127 at room temperature (pH 6) for 2 h, dialyzed against 100% ethanol, and lyophilized. The percent of total F127 PEO blocks cross-linked with ED was determined by ^{1}H-NMR (Fig.S1) by subtracting the peak area of protons at 3.12 ppm that represent the monovalent conjugation of ED to PEO blocks (Fig.S1B, peak 4) from the peak area of protons at 4.22 ppm (Table S1) that represent both the monovalent and divalent conjugation of ED to PEO blocks (Fig.S1B & C, peak 1A), dividing the difference by 4 (the area of the peak at 4.22 ppm [Fig.S1, peak 1A] expected at 100% ED cross-linking), and multiplying by 100. The peak representing monovalent ED conjugation (3.12 ppm) was not observed over this range of molar ratios. Average percent of total F127 PEO blocks cross-linked with ED ± SD (n=2 samples from the same batch) vs. molar ratio of ED/NHS-F127 was fit by a second order polynomial (dashed line) where $Y=B_0 + B_1X + B_2X^2$

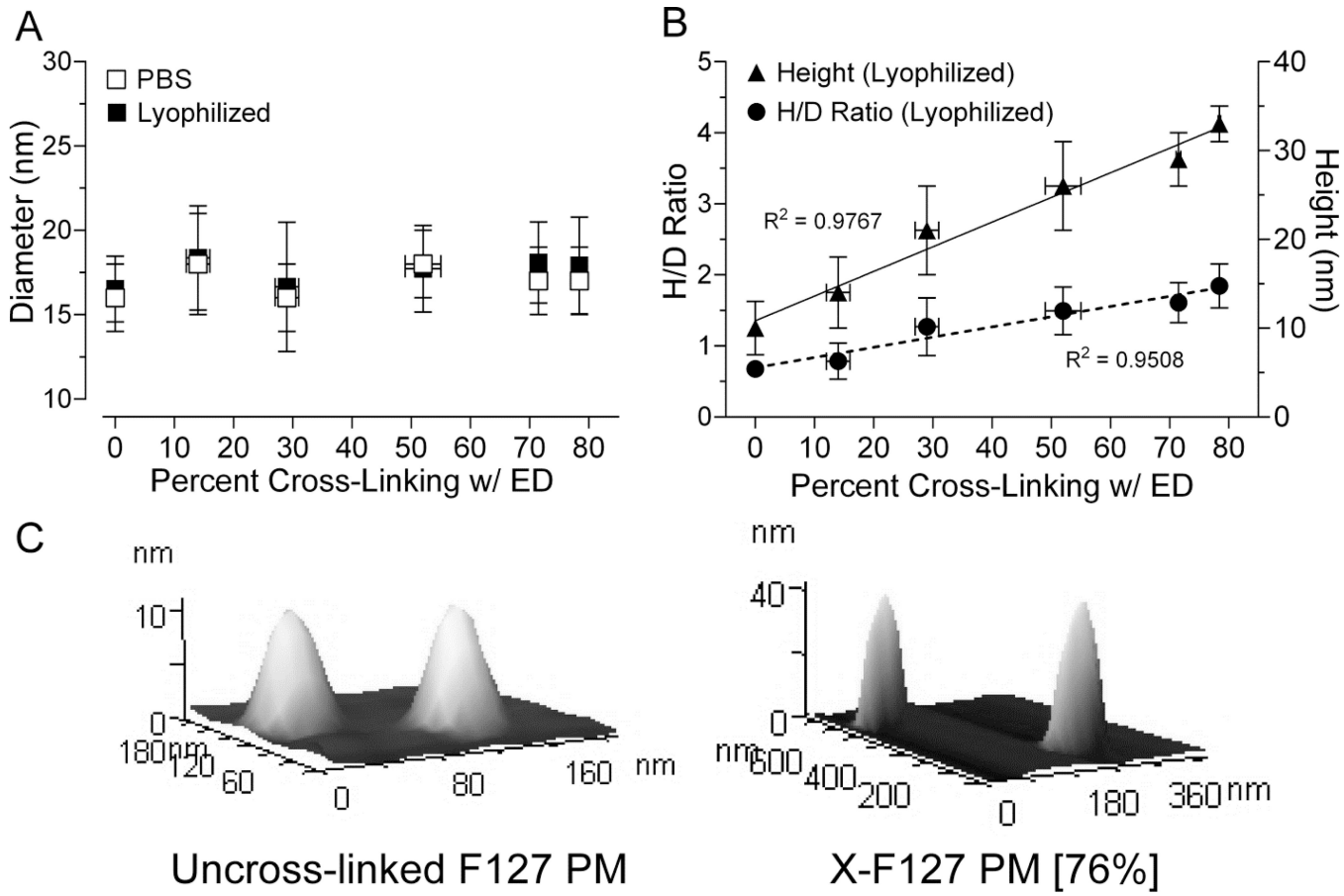

Fig.4.

Effect of increasing peripheral shell cross-linking on the size of Pluronic F127 PM in buffer and after lyophilization. (A) Lyophilized samples were measured by AFM (closed squares) or resuspended in PBS at 2 mg/mL, incubated at r.t. for 2 h, then measured by DLS (open squares). Average percent of total F127 PEO blocks cross-linked with ED ± SD on the X-axis were taken from Fig.3. The polydispersity of all samples in PBS ranged from 0.112 to 0.178 and larger peaks indicative of PM aggregation were not observed (data not shown). Average diameters after lyophilization ± SD (n=30) or resuspension in PBS ± SD (n=3 independent samples from the same batch) were compared by one way ANOVA with Tukey post-test. (B) Average heights (closed triangles, solid line) and height/diameter ratios (closed circles, dashed line) ± SD (n=30 micelles) of lyophilized samples were determined by AFM and fit vs. percent cross-linking with ED by linear regression. (C) Representative AFM images of uncross-linked F127 PM and F127 PM cross-linked with ED at 76% (X-F127 PM [76%]).

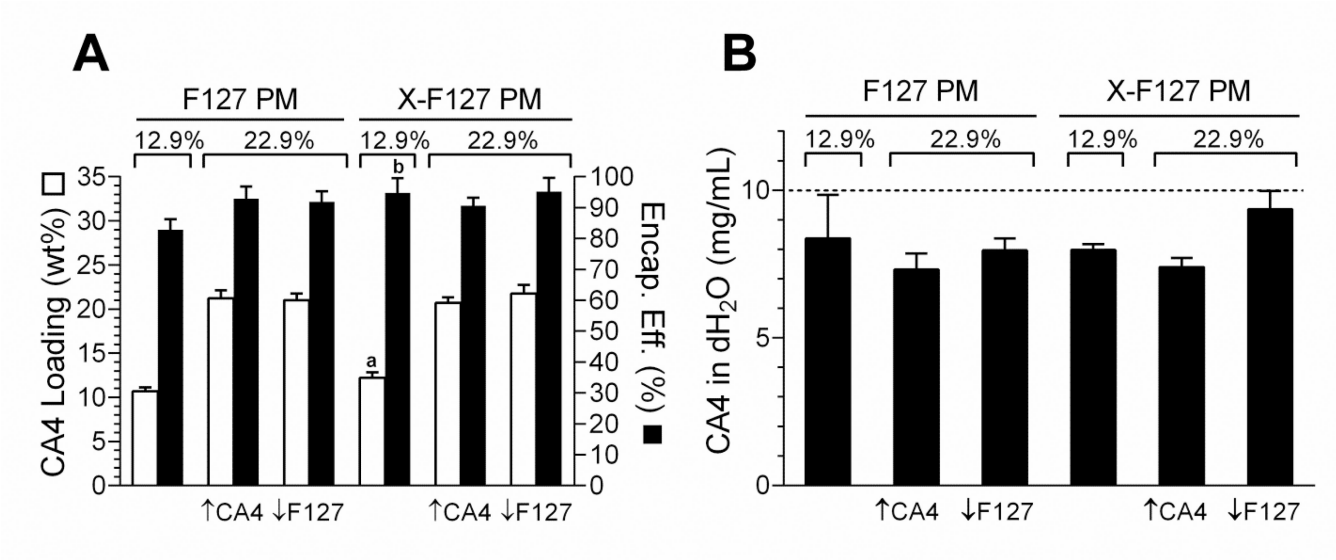

Fig.5.

Effect of peripherally cross-linking the shell of F127 PM on combretastatin A4 (CA4) loading and aqueous solubility. F127 polymer micelles alone (F127 PM) or F127 PM shell cross-linked with ED at 76% of total PEO blocks (X-F127 PM) were loaded with CA4 at 12.9 wt% or 22.9 wt% by the solid dispersion method and lyophilized. Theoretical loading of CA4 was increased from 12.9 wt% to 22.9 wt% by doubling the mass of CA4 (**↑CA4**) or using half the mass of F127 polymer (**↓F127**) in the solid dispersion. (A) Average CA4 loading (CA4 wt% of total formulation ± SD, n=3 from the same batch; open bars) and encapsulation efficiency (% of theoretical loading ± SD, n=3; closed bars) of the lyophilized samples were determined by LC-MS/MS and compared by student's t-test (P <0.05) at 12.9 wt% theoretical loading (P = ^{a}0.0255; ^{b}0.0251) or by one-way ANOVA with Tukey·s post-test at 22.9 wt% theoretical loading (P < 0.05). (B) Lyophilized formulations were resuspended in dH_2O at a theoretical concentration of 10 mg CA4/mL based on actual CA4 loading determined in (A). Average mg CA4 / mL dH_2O ± SD (n=3 independent samples from same batch) in the supernatants was determined by LC-MS/MS and compared to F127 PM at 12.9 wt% CA4 by one way ANOVA with Dunnet's post-test.

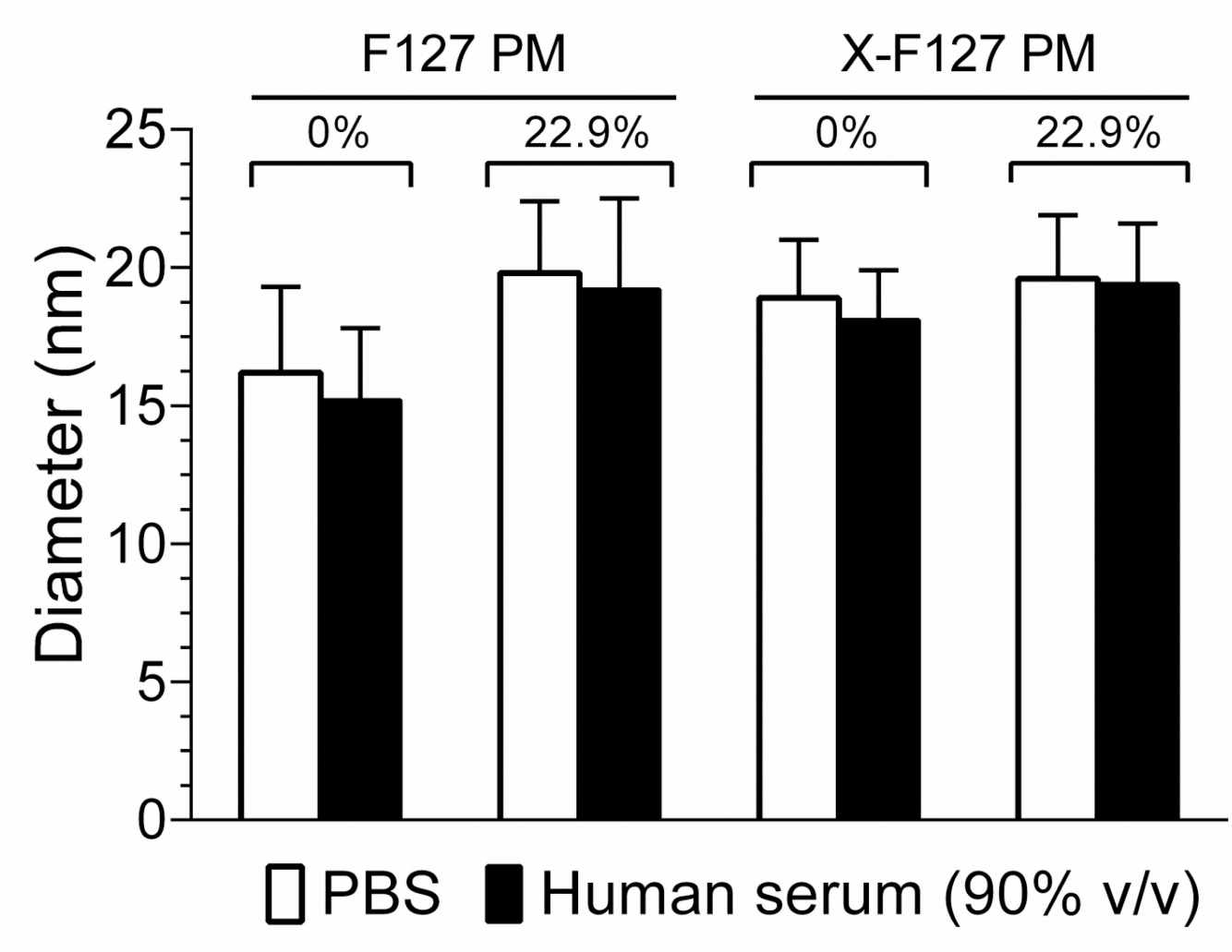

Fig.6.

Effect of peripherally cross-linking the shell of F127 PM on the hydrodynamic diameter in human serum. F127 polymer micelles alone (F127 PM) or individually cross-linked with ED at 76% of total PEO blocks (X-F127 PM) were loaded with CA4 at 22.9 wt% as described in Fig.5. Lyophilized formulations were resuspended in PBS, diluted to 2 mg/ mL in PBS (open bars) or human serum (90% v/v) (closed bars), and incubated at 37°C for 24 h. Average hydrodynamic diameters ± SD (n=3 independent samples from same batch) were then determined by DLS and compared by one way ANOVA with Tukey's post-test. The polydispersity index of the samples ranged from 0.143 to 0.269 and larger peaks indicative of PM aggregation were not observed (data not shown).

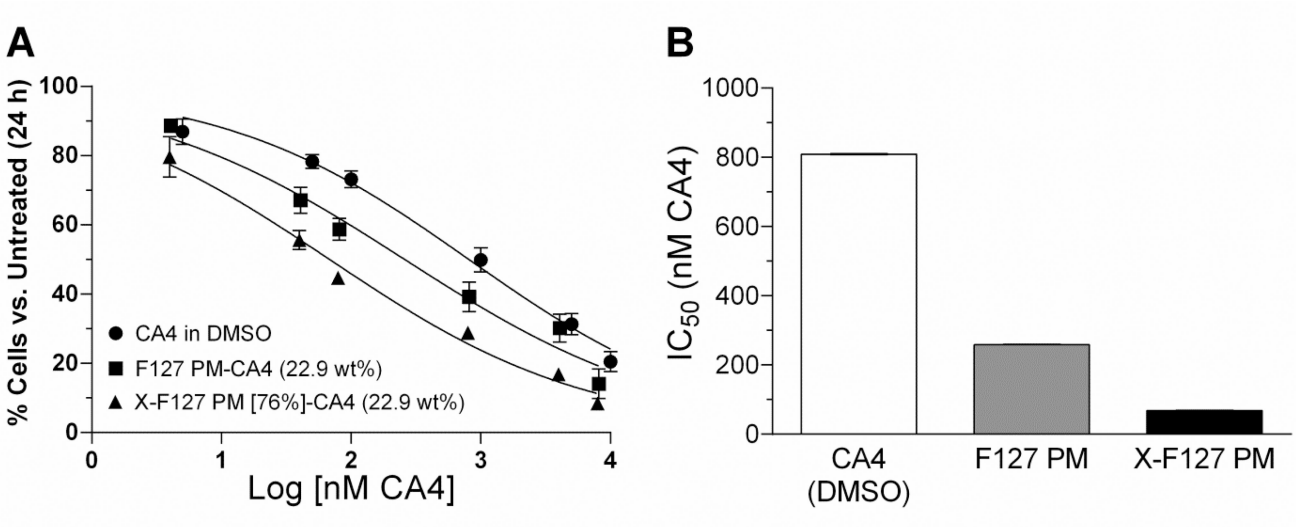

Fig.7.

Effect of peripherally cross-linking the shell of F127 PM on the potency of physically loaded CA4 against HUVEC growth. Uncross-linked F127 polymer micelles (F127 PM) or F127 PM individually cross-linked with ED at 76% of total PEO blocks (X-F127 PM) were loaded with CA4 at 22.9 wt% as described in Fig.5. (A) Subconfluent HUVEC were treated for 4 h with increasing concentrations of CA4 in DMSO (circles), CA4 loaded in F127 PM (squares), or CA4 loaded in X-F127 PM (triangles). After 24 h, the average % cell number ± SD (n=3) normalized to untreated HUVEC was determined by cell counting with trypan blue. Empty F127 or empty X-F127 PM at double the concentration present with 10 μM CA4 (20.8 μg / mL) did not affect HUVEC growth (data not shown). The extent of trypan blue exclusion for all treatment groups was similar to untreated HUVEC (~97%, data not shown). (B) The IC_{50} for CA4 in DMSO (open bar), CA4 in F127 PM (gray bar), and CA4 in X-F127 PM (closed bar) was calculated from the respective dose response curves by nonlinear regression using a variable slope. Standard error bars for the IC_{50} values are not visible on the bar graph.

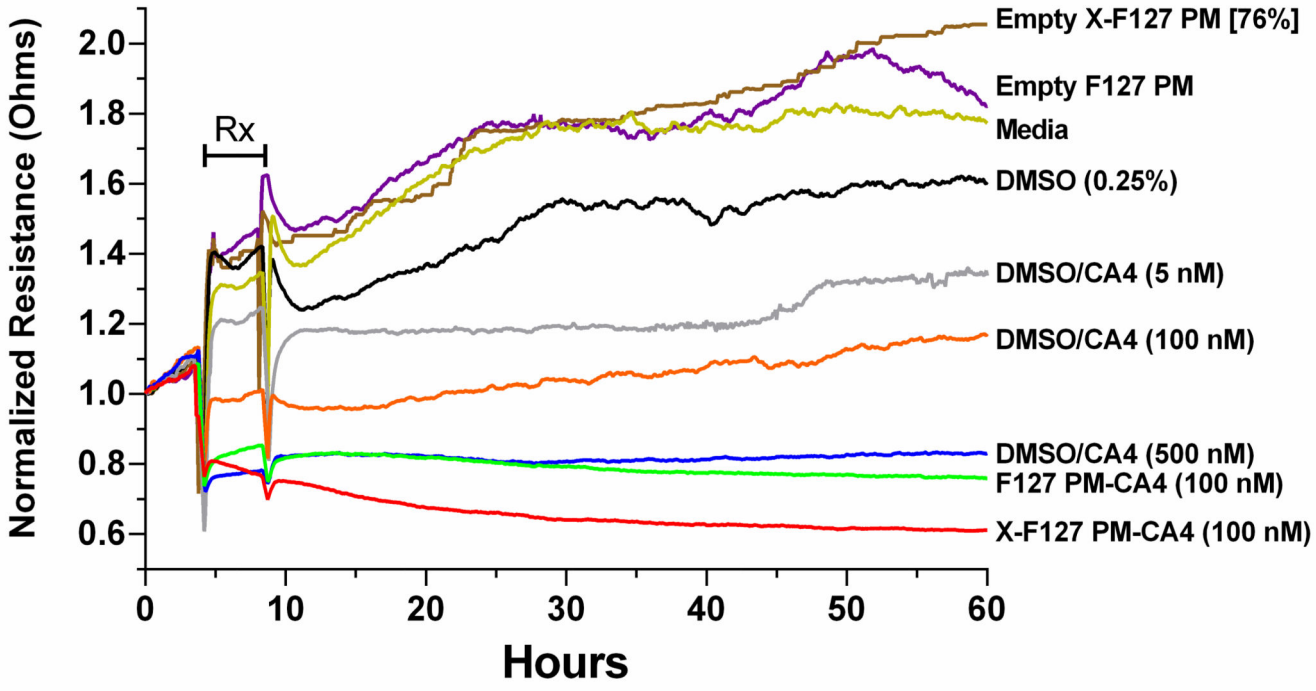

Fig.8.

Effect of peripherally cross-linking the shell of F127 PM on the activity of physically loaded CA4 against the well resistance of proliferating HUVEC monitored by electric cell impedance substrate (ECIS). CA4 was solubilized with 0.25% v/v DMSO or loaded in uncross-linked F127 polymer micelles (F127 PM) or F127 PM cross-linked with ED at 76% of total PEO blocks (X-F127 PM) at 22.9 wt% CA4 as described in Fig.5. Subconfluent HUVEC at densities equivalent to IC_{50} studies in Fig.7 were grown for 24 h and treated for 4 h ("Rx") with growth media (Media), empty F127 PM (0.1 μg/mL), empty X-F127 PM (0.1 μg/mL), or CA4 in the indicated formulation. Average well resistances (n=2 on each array) were normalized by dividing the resistance from treated wells by the resistance from wells with growth media alone using ECIS software.

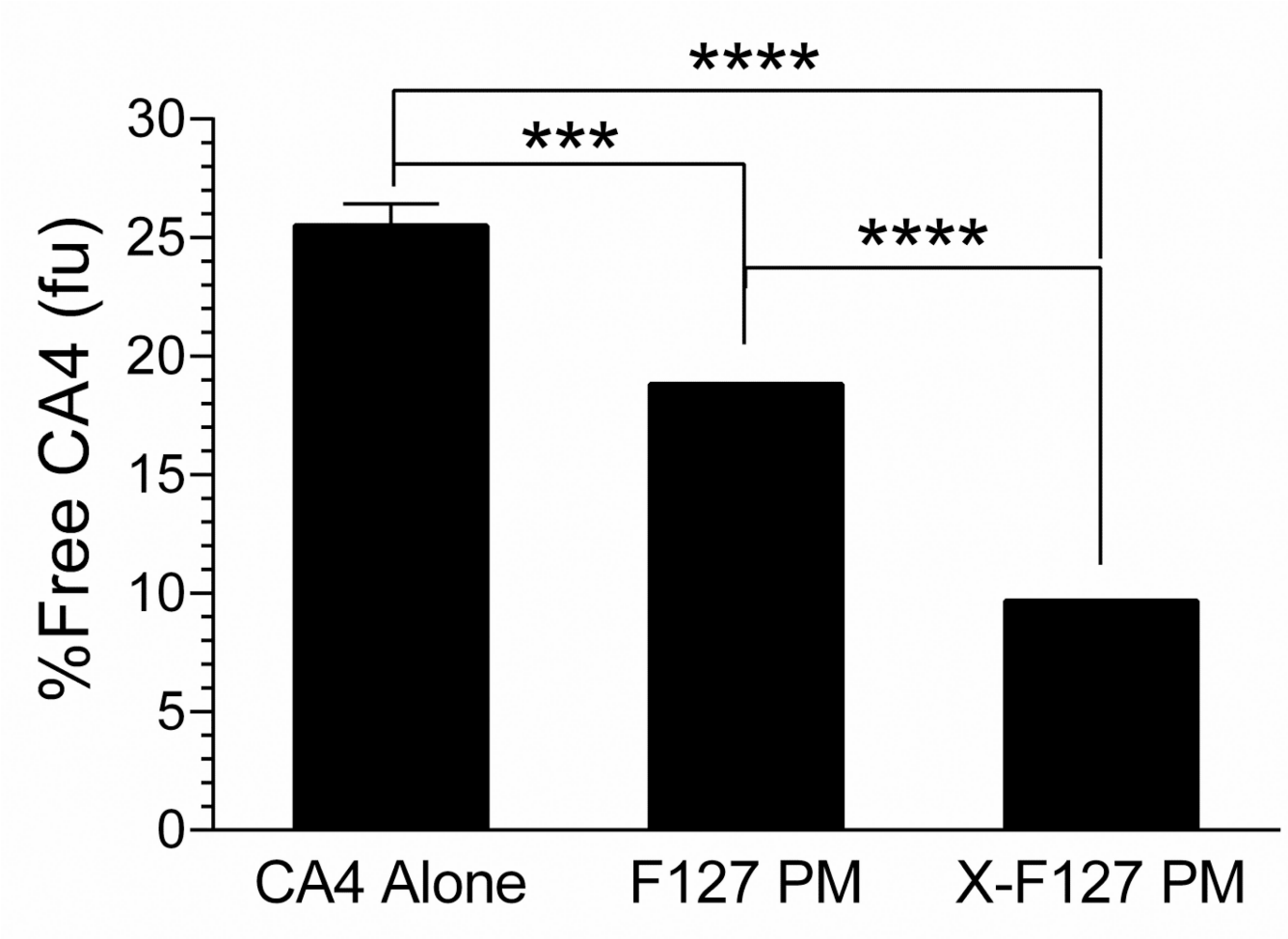

Fig.9.

Effect of peripherally cross-linking the shell of F127 PM on the unbound drug fraction of physically loaded CA4 in human blood (*fu*) at 37°C. F127 polymer micelles alone (F127 PM) or individually cross-linked with ED at 76% of total PEO blocks (X-F127 PM) were loaded with CA4 at 22.9 wt% as described in Fig.5. Lyophilized formulations were resuspended in dH_2O and analyzed by an erythrocyte vs. buffer or plasma partitioning method (pooled, whole human blood) at a concentration of F127 (0.057 mg F127/mL) below the CMC of F127 at 37°C (~0.189 mg F127/mL). Average % unbound fraction of CA4 (*fu*) ± SD (n=3 independent samples) after a 1 h incubation was determined by LC-MS/MS and compared by one way ANOVA with Tukey's post-test (***$P < 0.001$; ****$P < 0.0001$).

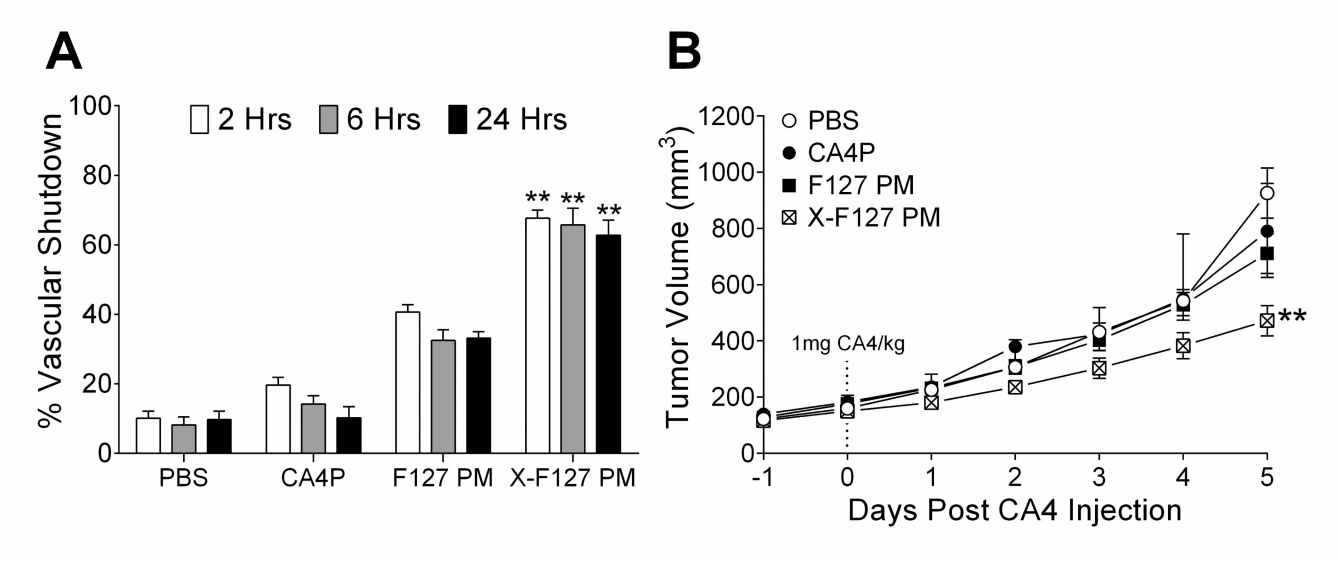

Fig.10.

Effect of peripherally cross-linking the shell of F127 PM on tumor vascular shutdown and subsequent growth inhibition by physically loaded CA4 after IV administration. F127 polymer micelles alone (F127 PM) or individually cross-linked with ED at 76% of total PEO blocks (X-F127 PM) were loaded with CA4 at 22.9 wt% as described in Fig.5. 4T1 cells stably expressing luciferase (4T1-Luc) were injected SQ into the mammary fat pad of female BALB/c mice and grown until ~100 mm^3 before treatment. (A) On the day of treatment, an average luciferase signal was obtained from the primary tumors before PBS, water-soluble CA4P, or CA4 loaded in F127 PM or X-F127 PM was injected IV (1 mg / kg). The average percent decrease in the initial luciferase signal ± SD (n = 6 mice) (% Vascular Shutdown) was then compared to PBS at the same time point by Kruskal-Wallis nonparametric ANOVA with Dunn's post-test ($^{a}P < 0.05$; $^{b}P < 0.01$; $^{c}P < 0.0001$). (B) Average tumor volumes ± SEM (n = 6 mice) after treatment with CA4P (closed circles), CA4 in F127 PM (closed squares), or CA4 in X-F127 PM (cross-hatched squares) were compared to PBS (open circles) on Day 5 post-CA4 injection by Kruskal-Wallis nonparametric ANOVA with Dunn's post-test (**$P < 0.01$).

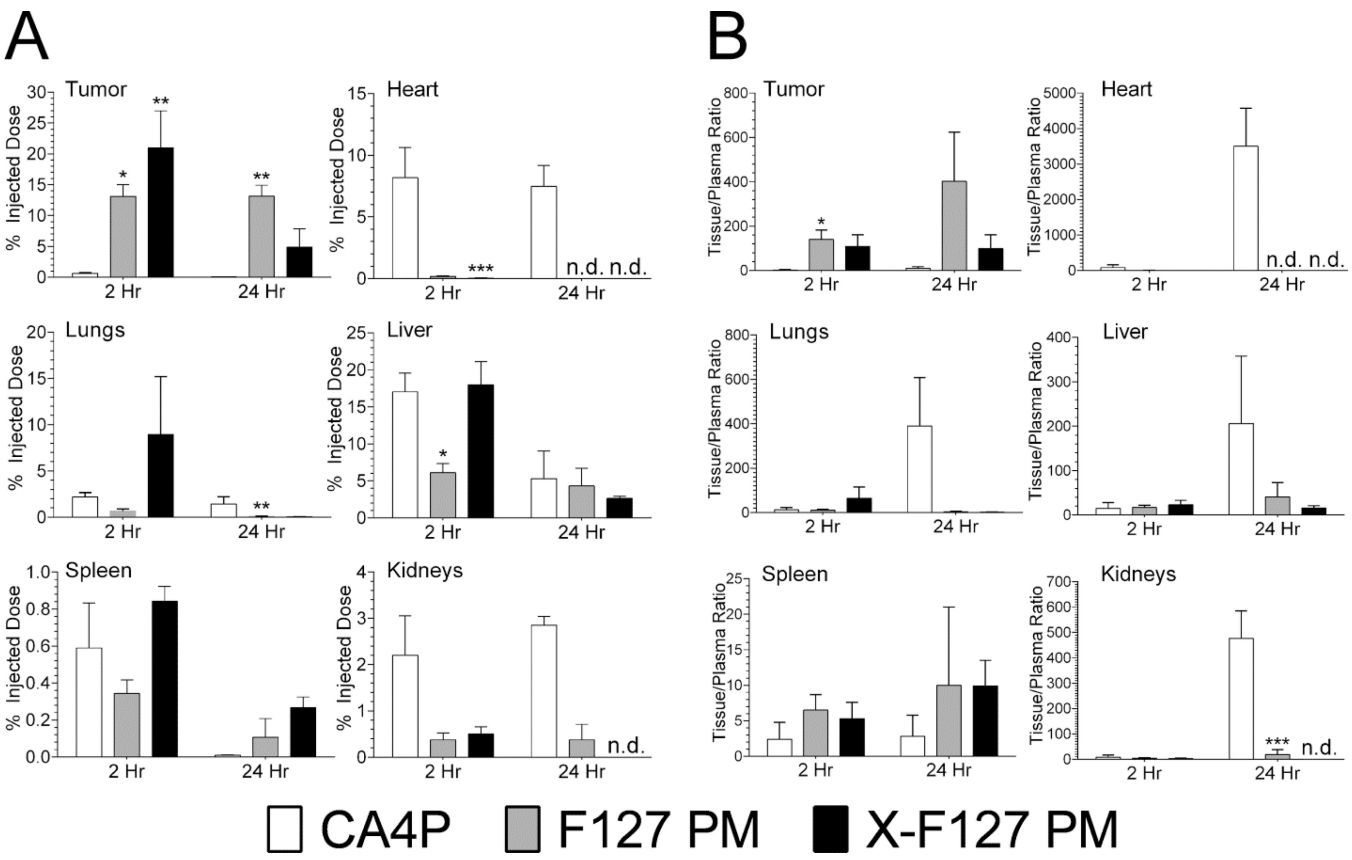

Fig.11.

Effect of peripherally cross-linking the shell of F127 PM on the distribution of physically loaded CA4 after IV administration in tumor-bearing mice. Uncross-linked F127 polymer micelles (F127 PM) or F127 PM individually cross-linked with ED at 76% of total PEO blocks (X-F127 PM) were loaded with CA4 at 22.9 wt% as described in Fig.5. 4T1 cells stably expressing luciferase (4T1-Luc) were injected SQ into the mammary fat pad of female BALB/c mice and grown until ~100 mm^3 before treatment. Water-soluble CA4P (open bars) or CA4 loaded in F127 PM (grey bars) or X-F127 PM (closed bars) was then injected IV (1 mg / kg) and the mass of CA4 / g tissue was determined by LC-MS/MS. (A) Average percent of injected dose ± SEM (n = 6 mice / time point) was determined from the mass of CA4 / g tissue and compared to CA4P at the same time point by Kruskal-Wallis nonparametric ANOVA with Dunn's post-test (*$P < 0.05$; **$P < 0.01$; ***$P < 0.001$). (B) Average issue to plasma ratios ± propagated SEM were calculated from data in A and drug plasma concentrations at the indicated time point from PK data in Table 1 and compared to CA4P at the same time point by one way ANOVA with Tukey's post-test (*$P < 0.05$; **$P < 0.01$; ***$P < 0.001$). n.d. – not detected.

Table 1

Pharmacokinetic parameters after IV administration (1 mg / kg) of water-soluble CA4P or CA4 physically loaded in uncross-linked F127 PM or F127 PM peripherally cross-linked with ethylenediamine at 76% (X-F127 PM) (22.9 wt% CA4) to female BALB/c mice bearing 4T1-Luc tumors as described in Fig.10 (n = 6 mice / time point).

PK Parameters	CA4P	F127 PM	X-F127 PM
AUC_{last} (h*ng/mL)	2531	3709	3702
$AUC_{0-\infty}$ (h*ng/mL)	2560	3990	4217
$MRT_{0-\infty}$ (h)	1.7	4.5	8
$t_{0.5}$ (h)	3.90	8.4	10.5
CL (L/h/kg)	0.39	0.25	0.24
V_{ss} (mL/kg)	0.67	1.1	1.9